Kent Academic Repository

Vitobello, Antonio, Mazel, Benoit, Lelianova, Vera G., Zangrandi, Alice, Petitto, Evelina, Suckling, Jason, Salpietro, Vincenzo, Meyer, Robert, Elbracht, Miriam, Kurth, Ingo and others (2022) *ADGRL1 haploinsufficiency causes a variable spectrum of neurodevelopmental disorders in humans and alters synaptic activity and behavior in a mouse model.* American Journal of Human Genetics, 109 (8). pp. 1436-1457. ISSN 0002-9297.

Downloaded from

https://kar.kent.ac.uk/95530/ The University of Kent's Academic Repository KAR

The version of record is available from

https://doi.org/10.1016/j.ajhg.2022.06.011

This document version

Author's Accepted Manuscript

DOI for this version

Licence for this version

UNSPECIFIED

Additional information

Versions of research works

Versions of Record

If this version is the version of record, it is the same as the published version available on the publisher's web site. Cite as the published version.

Author Accepted Manuscripts

If this document is identified as the Author Accepted Manuscript it is the version after peer review but before type setting, copy editing or publisher branding. Cite as Surname, Initial. (Year) 'Title of article'. To be published in *Title of Journal* , Volume and issue numbers [peer-reviewed accepted version]. Available at: DOI or URL (Accessed: date).

Enquiries

If you have questions about this document contact ResearchSupport@kent.ac.uk. Please include the URL of the record in KAR. If you believe that your, or a third party's rights have been compromised through this document please see our Take Down policy (available from https://www.kent.ac.uk/guides/kar-the-kent-academic-repository#policies).

ADGRL1 haploinsufficiency causes a variable spectrum of neurodevelopmental disorders in humans and alters synaptic activity and behavior in a mouse model

Antonio Vitobello[1,2,23,#], Benoit Mazel[1,2,3,23], Vera G Lelianova[4,5,23], Alice Zangrandi[5], Evelina Petitto[4], Jason Suckling[5], Vincenzo Salpietro[6] , Robert Meyer[7], Miriam Elbracht[7], Ingo Kurth[7], Thomas Eggermann[7], Ouafa Benlaouer[4], Gurprit Lall[4], Alexander G Tonevitsky[8], Daryl A. Scott[9], Katie M. Chan[9], Jill A. Rosenfeld[9], Sophie Nambot[1,3], Hana Safraou[1,2], Ange-Line Bruel[1,2], Anne-Sophie Denommé-Pichon[1,2], Frédéric Tran Mau-Them[1,2], Christophe Philippe[1,2], Yannis Duffourd[1,2], Hui Guo[10,11], Andrea K Petersen[12], Leslie Granger[12], Amy Crunk[13], Allan Bayat[14,15], Pasquale Striano[6,16], Federico Zara[6,17], Marcello Scala[6,16], Quentin Thomas[1,18], Andrée Delahaye[19,20], Jean-Madeleine de Sainte Agathe[21], Julien Buratti[21], Serguei V Kozlov[22], Laurence Faivre[1,3], Christel Thauvin-Robinet[1,2,18,23] and Yuri Ushkaryov[4,5,8,23,#]

1. *Inserm UMR1231 GAD, Génétique des Anomalies du Développement, Fédération Hospitalo-Universitaire Médecine Translationnelle et Anomalies du Développement (FHU TRANSLAD), CHU Dijon Bourgogne - Université de Bourgogne, Dijon, France*
2. *UF Innovation en diagnostic génomique des maladies rares, Centre Hospitalier Universitaire de Dijon, Dijon, France*
3. *Centre de Génétique et Centre de Référence Anomalies du Développement et Syndromes Malformatifs, FHU TRANSLAD - CHU de Dijon, Dijon, France*
4. *Medway School of Pharmacy, University of Kent, Chatham, United Kingdom*
5. *Department of Life Sciences, Imperial College London, London, United Kingdom*
6. *Department of Neurosciences, Rehabilitation, Ophthalmology, Genetics, Maternal and Child Health, University of Genoa, Genoa, Italy*
7. *Institute of Human Genetics, Medical Faculty, RWTH Aachen, Aachen, Germany*
8. *Faculty of Biology and Biotechnology, HSE University, Moscow, Russia*
9. *Department of Molecular and Human Genetics, Baylor College of Medicine, Houston, TX, USA*
10. *Center for Medical Genetics, School of Life Sciences, Central South University, Changsha, Hunan, China*
11. *Department of Genome Sciences, University of Washington School of Medicine, Seattle, Washington, United States of America*
12. *Randall Children's Hospital, Portland, Oregon, United States of America*
13. *GeneDx, Inc., Gaithersburg, Maryland, United States of America*
14. *Department of Epilepsy Genetics and Personalized Medicine, Danish Epilepsy Centre, Dianalund, Denmark*
15. *Department of Regional Health Research, University of Southern Denmark, Odense, Denmark*
16. *Pediatric Neurology and Muscular Diseases Unit, IRCCS Istituto Giannina Gaslini, Genoa, Italy*
17. *Medical Genetics Unit, IRCSS Istituto Giannina Gastini, Genoa, Italy*

18. *Centre de Génétique et Centre de Référence Déficiences Intellectuelles de causes rares, FHU TRANSLAD - CHU de Dijon, Dijon, France*
19. *UF médecine génomique et génétique clinique, Hôpital Jean Verdier, Hôpitaux Universitaires de Paris Seine Saint Denis, AP-HP, F-93140 Bondy, France*
20. *UFR de Santé Médecine et Biologie humaine, Université Sorbonne Paris Nord, F-93000 Bodigny, France and NeuroDiderot UMR 1141, Inserm, FHU I2-D2, Université de Paris, F-75019 Paris, France*
21. *Département de Génétique Médicale, Hôpital Pitié-Salpêtrière, AP-HP, Sorbonne Université, Paris, France*
22. *Center for Advanced Preclinical Research, National Cancer Institute, Frederick, United States*
23. *Equal contribution*

#Corresponding authors:

Dr Antonio Vitobello
University of Burgundy
15, Maréchal de Lattre de Tassigny,
21079 Dijon Cedex
France
Email: *antonio.vitobello@chu-dijon.fr*

Prof Yuri Ushkaryov
Medway School of Pharmacy
University of Kent
Anson Building, Central Avenue
Chatham, ME4 4TB
UK
Email: Y.Ushkaryov@kent.ac.uk

ABSTRACT

ADGRL1/latrophilin-1, a well-characterized adhesion G protein-coupled receptor, has been implicated in synaptic development, maturation and activity. However, the role of ADGRL1 in human disease has been elusive. Here, we describe 10 individuals with variable neurodevelopmental features including developmental delay, intellectual disability, attention deficit hyperactivity and autism spectrum disorders, and epilepsy, all featuring heterozygous variants in *ADGRL1*. *In vitro*, human *ADGRL1* variants expressed in neuroblastoma cells showed faulty ligand-induced regulation of intracellular Ca^{2+} influx, consistent with haploinsufficiency. *In vivo*, *Adgrl1* was knocked out in mice and studied on two genetic backgrounds. On a non-permissive background, mice carrying a heterozygous *Adgrl1* null allele exhibited neurological and developmental abnormalities while homozygous mice were non-viable. On a permissive background, the null allele also appeared at sub-Mendelian frequency, but many *Adgrl1* null mice survived the gestation and reached adulthood. The *Adgrl1*$^{-/-}$ mice demonstrated stereotypic behaviors, sexual dysfunction, bimodal extremes of locomotion, augmented startle reflex and attenuated pre-pulse inhibition, which responded to risperidone. *Ex vivo* synaptic preparations displayed increased spontaneous exocytosis of dopamine, acetylcholine and glutamate, but *Adgrl1*$^{-/-}$ neurons formed synapses *in vitro* poorly. Overall, our findings demonstrate that *ADGRL1* haploinsufficiency leads to consistent developmental, neurological and behavioral abnormalities in mice and humans.

Key Words: *ADGRL1*, Adgrl1 knockout mice, developmental delay, neuropsychiatric disorders, epilepsy

Introduction

G protein-coupled receptors (GPCRs) are seven-transmembrane cell-surface receptors that mediate a plethora of cellular responses to a variety of stimuli, regulate many important physiological functions and represent targets of 34% of all FDA-approved drugs.[1–5] The members of the adhesion GPCRs (aGPCRs) family interact with membrane-bound proteins, extracellular matrix components or soluble molecules and play a critical role in central nervous system development,[6–13] synapse formation,[14] myelination,[15] and immunity.[16] These receptors feature a distinctive structure composed of a large, adhesion-like N-terminal extracellular region containing a 'GPCR autoproteolysis-inducing' (GAIN) domain, and a signaling domain characterized by seven transmembrane helices with interconnecting loops and a cytosolic C-terminal tail. In most aGPCRs the GAIN-domain constitutively cleaves the receptor at the 'GPCR proteolysis site' (GPS) into N- and C-terminal fragments (NTF and CTF) that are non-covalently linked to each other at the cell membrane.[17–19]

The aGPCR latrophilin 1 (LPHN1 or ADGRL1) [*ADGRL1* MIM: *616416], also known as calcium-independent receptor of α-latrotoxin 1 (CIRL1), is considered to be a prototypical aGPCR, as its studies were seminal for the understanding of their structure and function.[6,18] It is a member of the ADGRL subfamily comprising three paralog members, ADGRL1-3/LPHN1-3 [*ADGRL2* MIM: *607018; *ADGRL3* MIM: *616417], and a structurally divergent member, ADGRL4/ELTD1 [*ADGRL4* MIM: *616419].[20] ADGRL1/LPHN1/CIRL1 was initially isolated and described because of its affinity for an exogenous ligand, α-latrotoxin (αLTX), the main neurotoxin of black widow spider venom. αLTX causes massive spontaneous neurotransmitter release via a complex mechanism involving the activation of several distinct receptors, with ADGRL1 playing a major role, and the insertion of tetrameric toxin complexes into the plasma membrane with subsequent pore formation.[21–25] The NTF of ADGRL1 (Figure 1A) has an adhesive function and consists of two adhesion modules, Lectin and Olfactomedin Domains, followed by a Hormone Receptor Motif adjacent to the GAIN domain, which cleaves the receptor. The CTF has a signaling function and a typical GPCR structure.[26] Although

ADGRL2 and 3 share extensive sequence similarity to ADGRL1, only ADGRL2 weakly binds αLTX, and all three are differentially expressed in tissues, which could reflect different functions.

It has been demonstrated that in the rat, the ortholog genes of human *ADGRL1* and *ADGRL3* are almost exclusively expressed in brain tissue, while *ADGRL2* is expressed in most tissues including liver, heart and kidney, albeit with a significant level of cerebral expression.[27,28] In humans, a similar expression pattern was observed, even though ADGRL1 protein was detected at low levels also in other non-neural tissues including heart, placenta, lung, liver, skeletal muscle, kidney and pancreas.[29] Alternative splicing of the NTF and CTF of ADGRLs, and their protein ligands, possibly contributes to the complexity of these interactions and the diversity of cellular responses.[27,29–33] In rat brain, *Adgrl1*, the most abundantly expressed paralog, appears at early postnatal stages and peaks at the age of 2-3 weeks.[26,27,29,31,34] Its expression is observed in all neurons, but not in glial cells, and is especially abundant in the cortex, hippocampus, dentate gyrus and cerebellum, with an expression pattern similar to that of many synaptic proteins, including another αLTX receptor, NRXN1/neurexin 1α [*NRXN1* MIM *600565].[35]

Several laboratories contributed to the untangling of the ADGRL1 interactome, showing its ability to bind a variety of ligands including teneurin transmembrane protein 2 (TEN2 -*TENM2* MIM *610119), neurexins 1α, 1β and 2β [*NRXN2* MIM *600566], fibronectin leucine rich transmembrane protein 1 and 3 (*FLRT1* MIM *604806, *FLRT3* MIM *604808), and contactins, and indicating its major role in regulating synaptic development and activity.[30,31,36–40] *Adgrl1* knockout (KO) in mice showed that this gene is apparently dispensable for embryonic development, with homozygous mutant mice demonstrating normal appearance, life span and fertility, but distinct synaptic physiology and inability to attend to their litters, a behavior that required further investigation.[39,41]

Few studies have so far directly implicated ADGRLs in human pathology, although this subfamily has been linked to several psychiatric, neurologic or neurodevelopmental conditions such as autism spectrum disorder (ASD), attention deficit and hyperactivity disorder (ADHD), bipolar disorder, schizophrenia, epilepsy, and substance use disorder (SUD).[26] Individuals harboring overlapping 19q13.12 microdeletions with a common critical region including five genes, most prominently *ADRGL1* and *PKN1* [MIM *601032], show intellectual disability, psychomotor and language delay, hearing impairment, brachycephaly, as well as a behavioral phenotype characterized by hyperactivity and stereotyped movements.[42] *ADGRL2* has been associated with brain and craniofacial development disorders.[43] A *de novo* heterozygous *ADGRL2* missense variant was identified in a fetus with extreme microcephaly, rhombencephalosynapsis and almost absent sulcation.[44] Authors hypothesized that this variant was responsible for an excessive neuronal cell adhesion, leading to this severe phenotype. *ADGRL3* polymorphisms have been associated with ADHD susceptibility and increased response to stimulant medication.[45–53] Temporal and spatial expression of this gene appeared relevant at the earlier stages of brain development and in brain regions known to be associated with ADHD. Multiple *ADGRL3* coding and non-coding variants within the gene or in nearby regulatory regions have been associated with variable severity ADHD phenotypes.[49,54] A large study of dyslexic families also showed an association between the chromosomal 4q13.1 region (encompassing *ADGRL3*) and dyslexia, by identifying a single nucleotide polymorphism (SNP) located 707 kb upstream of *ADGRL3*.[55] Recently, a significant association was observed between an *ADGRL3* SNP and susceptibility to early-onset ADHD and ASD in a large cohort of male individuals.[56]

However, to date, *ADGRL1* has not been clearly implicated in human disease, and behavioral phenotypes in *Adgrl1* KO mice remain unclear. Here, we present a series of ten individuals with rare variants in *ADGRL1* and provide molecular data demonstrating that their pathological functions are consistent with haploinsufficiency. Furthermore, we dissect the pathophysiological mechanisms leading to synaptic dysfunction in *Adgrl1* KO mice and provide a detailed characterization of the associated behavioral phenotypes. Overall, our data demonstrate that *ADGRL1* haploinsufficiency accounts for a spectrum of developmental, neurological and behavioral features.

Material and methods

Individuals, exome sequencing analysis and ethics statement

The procedures followed for genetic testing were in accordance with the ethical standards of the responsible committee on human experimentation and proper informed consent was obtained from all individuals. Individuals underwent exome sequencing as part of their care and several care providers were not required to obtain an institutional review board (IRB) approval to participate to this study. The protocols 2016-A01347-44 (Discovery), EK302-16 and SJ-91 were deployed by the CHU Dijon Bourgogne, the Uniklinik RWTH Aachen and the Ethics committee in region Sjaelland/Denmark respectively.

Publication of anonymized data from Individual 2 was approved by the institutional review board (IRB) of Baylor College of Medicine (Protocol H-47546). Individual 5 was already reported in *Guo et al., 2019*.[57] Consent for publication was obtained from all the other families.

Exome sequencing was performed as previously described (Supplemental information).[58]

All experimental procedures involving animals were approved by the Imperial College London and University of Kent Ethical Review Committees, and performed in accordance with the Animals (Scientific Procedures) Act 1986 and the European Convention for the Protection of Vertebrate Animals used for Experimental and Other Scientific Purposes.

Adgrl1 knockout in mice

To inactivate *Adgrl1* in 129/SvJ mice using homologous recombination in embryonic stem (ES) cells, a large fragment of mouse genome was first isolated from a mouse genomic library in a BAC vector (BACPAC Genomics, USA), using a 150-bp fragment of the *Adgrl*1 cDNA (which included exon 1) as a hybridization probe. Three BAC clones (120-150 kbp) containing overlapping fragments of *Adgrl1* were isolated, mapped and partially sequenced. To create a targeting vector for homologous recombination, a 12.8 kbp fragment of the gene, containing the promoter and exons 1-3, was subcloned into the pBlueScript plasmid. The 3.3 kbp intron between exons 1 and 2 (including small parts of these exons) was replaced with a neomycin (Neo) resistance gene under the 3-

phosphoglycerate kinase promoter (1.8 kbp), which disrupted the open reading frame and served as a positive selection marker. The Neo cassette was flanked by two loxP sequences for potential Cre-mediated excision and *Adgrl1* expression rescue. The vector also contained the gene encoding the A chain of diphtheria toxin (DTa) under the RNA polymerase II promoter, for negative selection against random incorporation of the whole vector into the ES cell genome. A linearized targeting vector was used to generate stably transfected 129/SvJ ES cell line. The successful homologous recombination was verified by Southern blot hybridization and PCR. Using ES cell clones, which carried the mutant *Adgrl1*$^-$allele, and standard transgenic techniques, chimeric 129/SvJ mice were generated. Mice transmitting the inactivated *Adgrl1* allele through the germline (strain designation AG148-2) were selected, inter-crossed, and then backcrossed to C57BL/6J mice (Charles River, UK). Mice from the colony maintained on the C57BL/6 background were used in most experiments.

Western blot analysis

Immediately after extraction, prefrontal cortices from wild-type, heterozygous and knockout mouse brains were used to prepare P2 membranes, as described previously.[59] The samples containing equal amounts of protein were dissolved in Sample Buffer, containing 2% SDS, 100 mM DTT, 60 mM Tris-HCl, pH 6.8, and 6% glycerol. To avoid irreversible precipitation of the CTF of ADGRL1 due to boiling in SDS, all samples were heated for 30 min at 50°C but never boiled. The samples were separated by electrophoresis in SDS-Tris-glycine gels containing 4% (for TEN2) or 8% (for all the other proteins) polyacrylamide (National Diagnostics, Atlanta, GA, USA). Separated proteins were blotted onto polyvinylidene fluoride membranes (Immobilon-P, IPVH00010, Merck) in Tris-glycine Transfer Buffer containing 20% methanol, at 100 V for 90 min (120 min for TEN2). The membranes were blocked in 5% fat-free milk and immunostained with the following primary antibodies: rabbit polyclonal antibodies against the NTF (RL1)[60] and the CTF of rat ADGRL1 (R4);[61] rabbit polyclonal IgGs against peptides from the NTFs of ADGRL1 (PAL1), ADGRL2 (PAL2), and ADGRL3 (PAL3);[62]a mouse polyclonal antibody against human TEN2 (dmAb, made in-house against the C-terminal amino acids 2412-2637 of LASSO, JF784343);[30]a rabbit polyclonal antibody against rat NRXN1α and β (#116; made in-house using the C-terminal peptide CSANKNKKNKDKEYYV);[61] a rabbit anti-V5 antibody (to stain the NTF of ADGRL1 variant constructs; Sigma-Aldrich, Cat# V8137, RRID: AB_261889); a mouse monoclonal antibody against β-actin (Abcam, Cambridge, UK). Prior to their use for immunostaining, some of these antibodies were affinity-purified, using the following procedures: (1) to purify RL1, R4, PAL1, PAL2, PAL3, and dmAb, ~100 µg of respective recombinant proteins expressed in NB2a cells were separated by SDS-gel electrophoresis, transferred onto Immobilon membranes, and incubated overnight with respective IgG fractions or the immune sera; the membranes were then washed with 25 mL of 1 M NaCl, the bound antibodies were eluted from the antigen with 50 mM triethylamine (pH 12) and neutralized with 1 M Tris-HCl, pH 8.3; (2) NRXN1 antibody was purified from the immune serum by affinity chromatography on the cognate peptide conjugated to SH-Sepharose. The blots were then incubated with respective secondary antibodies conjugated with horseradish peroxidase, followed by chemiluminescent detection using SuperSignalTM West Femto Maximum Sensitivity Substrate (Thermo Scientific) and the LAS3000 (FUJIFILM) gel documentation system. To determine the linear signal range for each protein, different signal development and detection times were used. For protein quantification the ImageJ software (NIH, Bethesda, MD, USA; RRID: SCR_003070) was employed.

Genotyping

Tail biopsies obtained from 21 day-old mice (or tissue fragments of partially cannibalized newborns) were used to extract genomic DNA. Two PCR-amplification reactions were set up for each sample and included 1 µg of genomic DNA and one of the two primer pairs (Figure S2A): N252 (5’-AGG CCG TGG TAC CCT GGT GAT GCG GGG CGA GG) and N253 (5’-GCG TGT GCA GGA TCC CAG GCC AGA GCC GGG TAA TTA CTT GTT TT), or N252 and N255 (5’-CGA GAC TAG TGA GAC GTG CTA CTT CCA TTT GTC), which were specific for the WT or KO *Adgrl1* allele and produced amplification fragments of 522 and 459 bp, respectively. Hot-start PCR reactions were performed on a Mastercycler (Eppendorf, UK), using the following program: initial denaturation (10 min at 94 °C), 34 cycles of amplification (60 s denaturation at 94 °C, 90 s annealing at 60 °C, 45 s extension at 72 °C) and final extension (10 min at 72 °C). The PCR products were analyzed by agarose gel electrophoresis.

Neuronal cell cultures

Hippocampi from 1 day old mice were dissected under a binocular microscope in aseptic conditions, placed into vials with HAB buffer (Hibernate A, 2% B27, 0.5 mM GlutaMAX) and kept at 4°C until plating (no later than 10 days after dissection). The hippocampi were placed in dissociation buffer (Hibernate A without Ca^{2+}, containing 2 mg/ml papain) and incubated 10 min at 37°C. The buffer was then replaced with HAB buffer and the tissue was triturated using a silanized Pasteur pipette. This undispersed pieces were let to settle for 1 min, the supernatant containing the dispersed cells was transferred into a 15 ml tube and centrifuged at 700 rpm for 2 min. The pellet was resuspended in Neurobasal A medium supplemented with 2% B27 and 0.5 mM GlutaMAX, and the cells were plated at a density of 10,000 cells/well on coverslips precoated with 50 µg/ml poly-D-lysine and 10 µg/ml laminin and placed into 24-well plates. Neurons incubated at 37°C, 5% CO_2 and half of the medium was changed every 3-4 days. The cultures were maintained until 60 days in vitro (DIV) and used for electrophysiological recordings at different times.

Synaptic activity in cultured hippocampal neurons

Recordings of spontaneous postsynaptic currents in hippocampal neurons were carried out after 14-60 DIV. Coverslips with neurons were transferred into a perfusion chamber (Harvard Biosciences, Inc.) mounted on the stage of an inverted microscope and perfused at room temperature with the continuously oxygenated External solution (2 mM $CaCl_2$, 3 mM CsCl, 11 mM glucose, 4.8 mM HEPES, pH 7.4 adjusted with NaOH, 160 mM NaCl, 1 µM tetrodotoxin) at a flow rate of 1 ml/min. Patch pipettes were prepared from filamented borosilicate glass capillaries (Harvard Biosciences, USA) to achieve a DC resistance of 3 – 7 MΩ and filled with the Internal solution (150 mM CsCl, 10 mM EGTA, 5 mM HEPES, pH 7.4 adjusted with KOH, 10 mM NaCl, 4.5 mM ATP-Mg, 0.1 mM GTP). Cells were observed using a color video camera and pipettes were positioned using a PatchStar motorized micromanipulator (Scientifica, UK). The recordings were carried out in the whole-cell configuration, on cells voltage-clamped at -70 mV. To block Current signals were amplified (10 mV/pA), filtered at 2.9 kHz and digitized at 20 kHz using a recording system including a Model 2400 patch-clamp amplifier (A-M Systems, Inc., USA), an LPF202A filter/amplifier (Warner Instruments, USA), a HumBug harmonic frequency quencher (Quest Scientific, USA) and a Digidata 1322A digitizer (Axon Instruments, USA). Data acquisition was controlled using pClamp (Axon Instruments) and the traces were analyzed with MiniAnalysis (Synaptosoft, USA)

Synaptic activity at the NMJ

Flexor digitorum brevis muscles were dissected from P21 mice (*Adgrl1*$^{+/+}$ or *Adgrl1*$^{-/-}$) and pinned to the bottom of Petri dishes coated with Sylgard (Dow Corning). In this set of experiments, we systematically tested male mice to avoid any effects of the estrous cycle; however, several experiments conducted on adult females in metestrus produced similar results. The recording buffer contained: 137 mM NaCl, 5 mM KCl, 2 mM $CaCl_2$, 1 mM $MgCl_2$, 10 mM HEPES, pH 7.4, 5.6 mM glucose, 1 µM tetrodotoxin. Sharp electrodes were manufactured from borosilicate glass (Harvard Biosciences) with a tip diameter <0.5 mm and ~70 MOhm impedance, and filled with a 5 M ammonium acetate solution. Spontaneous presynaptic activity was recorded using an Axoclamp 2B pre-amplifier (Axon Instruments) in the current clamp mode, an LPF202A secondary filter/amplifier, a HumBug harmonic frequency quencher, a Digidata 1322A digitizer and a microcomputer running AxoScope software (Axon Instruments). The recorded signals were analyzed using MiniAnalysis.

Loss of righting reflex

The righting reflex was tested between postnatal days P3 and P10. No pre-test learning was required. Pups were gently held on their backs on a flat surface for 5 s and then released. The time required for the pup to return to prone position was recorded in three trials, each of which lasted up to 60 s.

Locomotor activity and stereotypy

WT, HET and KO mice aged 2–6 months were housed individually with food and water provided *ad libitum*. Cages were fitted with running wheels, whose revolutions were recorded in 1-min bins and analyzed using the Chronobiology Kit (Stanford Software Systems, Santa Cruz, CA, USA). Before commencement of experiments, mice were kept under a 12:12 h light-dark cycle for a minimum of 14 days and the same regime was maintained during the experiments. Environmental room lighting consisted of white fluorescent strip lights providing 350 lux at cage level.

Stereotypic behaviors (grooming, excessive jumping, tonic immobility, excessive digging etc.) were observed and timed for 10 min after mice were individually transferred into new cages.

Pre-pulse inhibition

The acoustic startle response apparatus was designed in-house and consisted of an acoustically insulated 35x35x35 cm chamber equipped with a ventilation system and a test platform. The latter included a plastic tubular rodent holder (Kent Scientific Corporation, USA) magnetically positioned on a 14x18 cm plastic plate, which rested on a piezoelectric force transducer (MLT1010, ADInstruments, Australia) attached to a heavy base; the transducer was used to detect animal motion inside the holder. Broad-band acoustic stimuli and background noise (BN) were delivered via two speaker drivers placed 5 cm above the animal holder and connected to a computer-controlled audio amplifier. Acoustic signal patterns for various trials were designed and replayed using the Audacity software (Audacity Team, USA) and calibrated to the required sound intensity using a sound level meter (815, Testo, Germany) placed near the animal holder. A BN was maintained in the chamber at 60 dB during the experiment. Animals were habituated to the experimental conditions in preliminary sessions that included no acoustic stimuli. Test experiments were designed according to previously published studies and consisted of 5 min acclimatization, followed by 10 no-prepulse/startle (NS) trials, then by a random series of 3 prepulse/startle (PS) trials, 5 NS trials and 5 no-prepulse/no-startle (NN) trials, then by another 10 NS trials.[63–66] All trials were interspaced by 15-s BN intervals, and consisted of the following segments: 100 ms BN; 20 ms pre-pulse (75 dB, 15 dB above BN) or BN;

100 ms interstimulus interval; 40 ms startle stimulus (120 dB, 60 dB above BN) or BN; 300 ms response period. Animal motion signals from each trial were rectified, digitized at 1000 Hz and recorded using a PowerLab data acquisition system (ADInstruments, Australia). Startle responses were quantified by calculating the area under response curves (AOC). Risperidone (1 mg/kg body weight, in 150 µL) was administered intraperitoneally 30 min prior to the PPI test; control mice were injected with vehicle; each mouse was used only once.

Neurotransmitter release from central synapses

Synaptosomes were prepared from prefrontal cortices of mouse brains as described previously and resuspended in physiological buffer (140 mM NaCl, 5 mM KCl, 1 mM $MgCl_2$, 10 mM glucose, 20 mM HEPES, pH 7.3) at a concentration of 1 mg protein/ml.[67] To measure spontaneous and evoked release of dopamine and noradrenaline, the synaptosomes were first equilibrated in physiological buffer supplemented with 2 mM Ca^{2+}, 1 mM ascorbic acid and 0.1 mM pargyline (Sigma-Aldrich, UK) for 10 min, at 37°C. The synaptosomes were then incubated with 2.5 µCi [7,8-^{3}H]-dopamine or [7,8-^{3}H]-noradrenaline (Amersham, UK) as outlined.[67] For glutamate loading, synaptosomes basal buffer containing 2 mM Ca^{2+} and 0.1 mM aminooxyacetic acid (Fisher, UK) were preincubated for 10 min, at 37°C, then supplemented with 2-5 µCi/ml [^{14}C]-glutamic acid (Amersham, UK) for 5 min, washed, resuspended in buffer with 2 mM Ca^{2+} and incubated for 1 h, at 37°C, washed and used to measure release. All buffers used to prepare synaptosomes and study release were oxygenated. Release of neurotransmitters was determined in multiple identical experiments, each involving triplicate samples of 25 µg loaded synaptosomes/experimental point.

Recombinant ADGRL1 constructs

The variant ADGRL1 expression constructs were created on the basis of rat *Adgrl1* (O88917) in the pcDNA3.1 vector, using a site-directed mutagenesis system (NEBaseChanger, New England Biolabs) and the following primer pairs: p.Trp9*, TGCAGCACTCT**A**GAGTCTCTGTGTGACGAC, GCCAAGCGGGCCATGGCG (annealing temperature, Ta, 72°C); p.Tyr346Cys,

CCGCGTGGACT**G**TGCCTTTAACA, TTGCCTGCTGCCTCACTG (Ta, 69°C); p.Trp1005Arg, CTATTTCATC**A**GGAGCTTCATTGGG, TTATCCACCCTCAGCCAG (Ta, 62°C); p.Met1152Thr, AATCCGGAGGA**C**GTGGAATGACAC, CGGCTCTGGGTCCCTGTG (Ta, 67°C); p.Ser1164Phe, GACAGAGTCGT**T**CTTTATGGCAG, TGCTTCCTCACGGTGTCA (Ta, 64°C). The correct base substitutions were confirmed by DNA sequencing. To obtain stable cell lines expressing these constructs, NB2a neuroblastoma cells were transfected using Escort III (Sigma-Aldrich) with WT *Adgrl1* (positive control), its variants (described above) or an empty vector (negative control), and selected using Geneticin (Thermo Scientific, UK).

Measurements of cytosolic Ca^{2+}

ADGRL1 expressed in neuroblastoma cells is known to react to the binding of LTX^{N4C} by triggering the intracellular Ca^{2+} signaling cascade.[68,69] To monitor cytosolic Ca^{2+} changes, a fluorescent Ca^{2+} indicator dye was used as described previously.[68,69] When stimulating ADGRL1 with toxin, it was important to use the mutant LTX^{N4C}, which does not form membrane pores and thus allows to study the receptor-mediated signals only.[25,70] As a positive control of LTX^{N4C}-induced Ca^{2+} signaling, the WT *Adgrl1* was used; two negative controls were employed: cells transfected with an empty vector and stimulated with LTX^{N4C}, and ADGRL1-expressing cells stimulated with buffer. Cells were grown in Dulbecco's Minimal Essential Medium (DMEM) containing 10% fetal bovine serum (FBS) and L-glutamine in 30 mm dishes to a required density. One day prior to the experiment, the medium was replaced with serum-free DMEM. The cells were then incubated in the dark with physiological buffer containing 0.2 mM EGTA, 0.5 mg/ml BSA, 2.5 mM Fluo-4 acetomethoxy ester (Fluo-4-AM, Thermo Fisher Scientific) and 10% Pluronic F-127 for 30 min, washed and further incubated for 30 min to allow for dye de-esterification. The cells loaded with the fluorescent dye were observed under a confocal microscope (LSM510, Zeiss United Kingdom), using a 40x Achroplan water-dipping objective, a 488 nm laser and a 505–550 nm band-pass emission filter. Confocal images were acquired every 5 s for the duration of the experiment which typically lasted 55-60 min, according to the following protocol: (1) baseline fluorescence (F_0) was initially recorded. (2) After 5 min recording, 1 nM LTX^{N4C} (or control buffer) was added in the absence of Ca^{2+}_e, to avoid asynchronous signaling while the receptors are independently activated in individual cells (this allowed toxin to bind and activate the receptors without inducing Ca^{2+} signals).[68] (3) At 30 min, Ca^{2+} was added to a final concentration of 2 mM, to induce synchronous receptor signaling. (4) At 50 min, 1 nM WT αLTX was added, to identify all cells able to bind the toxin and measure the maximal Ca^{2+} fluorescence (F_{max}) of each individual cell by inducing Ca^{2+}-permeable pores in them. (6) The recording continued for another 5 min. The fluorescence profile of each cell was adjusted to the baseline drift using controls and normalized between the specific F_0 and F_{max}.

Immunostaining of cultured hippocampal neurons

Neuronal cultures on glass coverslips were fixed with 4% paraformaldehyde/1% glutaraldehyde, quenched with 0.7 M Tris, blocked with 10% goat serum and then incubated overnight with rabbit anti-VGAT or mouse monoclonal anti-VGLUT antibodies (ThermoFisher Scientific, UK), at 4°C, before being stained for 1 h with Alexa Fluor 488-conjugated anti-rabbit or Alexa Fluor 568-conjugated anti-mouse secondary antibodies (ThermoFisher Scientific). The coverslips were mounted on glass slides and imaged under the LSM-510 confocal microscope using a Plan-Neofluar 40x/1.3 oil-immersion objective.

Statistical analysis

The data were initially assessed using a Lillefors normality test, and normally distributed sets of data were compared using a one-way ANOVA, with the Bonferroni correction for multiple pairwise comparisons where necessary. Non-normally distributed data were compared using a Wilcoxon (Mann-Whitney) non-parametric test for unpaired data. For binomial distributions, Jeffreys 95% and 99% confidence intervals were calculated. The level of statistical significance was set at $p = 0.05$ and the following indicators of probability levels were used throughout the paper: *, $p < 0.05$; **, $p < 0.01$; ***, $p < 0.001$. All data in the Figures are the means ± SEM. In behavioral experiments, littermates or age-matched mice were used, and the experimenter was always blind to mouse genotype.

Results

In an 8-year-old boy with a neurodevelopmental disorder, including mild to moderate intellectual disability, global developmental delay and behavioral disorders (Individual 1 – F1-II-1, Figure 1; Table 1 and Supplemental information) we performed array-comparative genomic hybridization (CGH) and trio exome sequencing (ES) and identified a *de novo* heterozygous missense variant (NC_000019.9:g.14267505A>G; NM_001008701.2:c.3013T>C; p.Trp1005Arg) in *ADGRL1*. No additional candidate single nucleotide, indel or copy number variants accounting for his phenotype were identified. *ADGRL1* is mainly expressed in the brain (The Human Protein Atlas, https://www.proteinatlas.org) and is highly intolerant to loss-of-function (LoF) and to missense variants according to gnomAD (v2.1.1), with a probability of LoF intolerance (pLI) of 1 and a missense Z (misZ) score of 3.43.[71] There were only 12 high-confident LoF alleles in gnomAD, all at the heterozygous state with a frequency ranging from $9.95x10^{-5}$ to $8.81x10^{-6}$ in ethnically matched allele counts. The p.Trp1005Arg variant is absent in gnomAD database (see Online database) and located within the CTF of the ADGRL1 protein, in a position highly intolerant to substitutions (Figure S1 – Metadome score 0.5). Furthermore, two individuals with *de novo* missense variants (NC_000019.9:g.14273591T>C – p.Tyr346Cys and NC_000019.9:g.14271102C>G – p.Ser546Thr) and ASD were reported in a meta-analysis cohort a of 3,871 autism cases and 9,937 ancestry-matched or parental controls (Figure S1A)[72].

Through international data sharing (GeneMatcher, ERN-ITHACA and personal collaborators), we ascertained nine additional individuals from eight unrelated families, with congruent phenotypes and *de novo* or inherited heterozygous candidate *ADGRL1* variants (Table 1, Figure 1), namely four nonsense (among which one previously included in Guo et al., 2019),[57] one frameshift and four missense variants (Table 1, Figure 1A, Figure S1B). Seven of them were *de novo*, while two, p.Trp278* and p.Try346Cys, were inherited from an affected parent with intellectual disability and learning difficulties (Families F3 and F9 respectively, Figure 1). In the p.Trp278* family, the variant segregated in six affected cases (F3 - Figure 1B), but only two individuals (i3 and i4, F3-II-5 and F3-II-6 respectively) were available for clinical evaluation. In the p.Tyr346Cys family (F9), the variant co-segregated with a pathogenic *TAOK1* variant [Developmental delay with or without intellectual impairment or behavioral abnormalities – autosomal dominant MIM 619575] in three affected cases (Figure 1B), but only one individual (i10, F9-II-2) was available for clinical evaluation.

Retrospective phenotyping of the ten individuals of our cohort delineated a consistent neurodevelopmental disorder characterized by global developmental delay, intellectual disability, ASD and/or ADHD. Age in the cohort ranges from 3 to 43 years (median age: 11 years). Nine presented with a developmental delay including poor motor skills and speech delay. Among them, two benefited from a significant psychomotor catch-up during their development (individuals 6 and 8). Walking acquisition age ranged from 11 to 30 months (median age: 16.5 months) while first pronounced words age ranged from 12 to 36 months (median age: 14.5 months).

Five individuals presented with mild to moderate intellectual disability, one presented with a borderline intelligence quotient (IQ, individual 7 – Figure 1C) and three had average IQs. Individual 2 (F2-II-1, Figure 1) was 3 year and 3 month-old at last consultation, therefore too young for a neuropsychological assessment. Five underwent brain imaging which was unremarkable except for individual 6 who showed bilateral focal nodular heterotopias of the frontal horns of the lateral ventricles.

In our cohort, 5/9 individuals presented with neuropsychiatric disorders (detailed clinical data were unavailable for individual 2). Among them, three matched diagnosis criteria for ADHD and four for ASD ranging from atypical autism to Asperger syndrome. Two individuals met the criteria for both ASD and ADHD (individuals 1 and 3, F1-II-1 and F3-II-5 respectively, Figure 1) and individual 5 (F4-II-1, Figure 1), presenting with Asperger syndrome, also presented with hyperactivity, impulsivity, inattention, and executive functioning deficits, which was strongly suggestive of ADHD. Stereotypies were present in two cases.

Epileptic features with EEG abnormalities were present in 2/9 individuals: individual 7 (F6-II-1, Figure 1) presented focal hypermotor seizures with secondary generalization to tonic-clonic seizures; individual 8 (F7-II-1, Figure 1) presented developmental delay and behavioral abnormalities at 5 years with the diagnosis of epileptic aphasia. His EEG revealed bilateral, asynchronous slow and spike waves on the central and posterior regions. He was prescribed carbamazepine (15 mg/day) with an effect on both EEG abnormalities and speech problems. Additional neurological features included inconstant hypotonia (4/9). No spasticity or ataxia was noted in the cohort.

Facial dysmorphism was observed in 7/10 cases but individual 2 (F2-II-1, Figure 1) presented with frontonasal dysplasia probably not linked to the *ADGRL1* variant. Dysmorphic features included broad nasal tip, deep philtrum, thin upper lip and donwslanted palpebral fissures. Macrocephaly (i.e., head circumference above 2 standard deviations of the 97th percentile) was present in 4/6 individuals with available data.

Other findings include sleep disturbance (5/9) such as non-organic insomnia (3/5) and nocturnal awakenings (2/5), mild extremity anomalies (3/9), overweight (4/9), joint hypermobility (4/8), dermatological issues (2/9), hyperphagia (2 individuals from the same family), anxiety (1/9), megadolichocolon (1/9), hyperopia (1/9), genital anomalies (1/9), delayed puberty (1/9), scoliosis (1/9), migraine (1/9), neuroendocrine pancreatic tumors (1/9). Overall, our data indicated that *ADGRL1* should be considered as a candidate gene for a neurodevelopmental disorder including ASD and ADHD with variable spectrum.

To understand the pathophysiological mechanisms underpinning the *ADGRL1* variants identified in our cohort, we produced *Adgrl1* constructs carrying the following variants: p.Trp9*, p.Tyr346Cys, p.Trp1005Arg, p.Met1152Thr and p.Ser1164Phe, and expressed them in mouse neuroblastoma cells. As shown in Figure 2A, four variant constructs were relatively well expressed, while the p.Trp9* construct produced no protein, indicating that this variant introduces a functional premature stop codon. Delivery of the expressed proteins to the cell surface was assessed using αLTX and anti-LTX antibodies. As expected, the cells expressing p.Trp9* showed no detectable αLTX binding (Figure 2A, B), whereas the p.Tyr346Cys- and p.Trp1005Arg-expressing cells bound the toxin proportionately to the amount of protein produced (Figure 2A, B). Interestingly, the two constructs with variants in the intracellular tail of the CTF (p.Met1152Thr and p.Ser1164Phe) bound substantially less toxin (Figure 2A, B). As αLTX only binds to the extracellular NTF, this result was likely due to inefficient delivery of the p.Met1152Thr and p.Ser1164Phe constructs to the cell surface, and this was confirmed by labeling of the surface-exposed ADGRL1 proteins with a membrane-impermeable biotin reagent and subsequent staining with streptavidin (Figure 2A, right).

Physiological activity of the ADGRL1 variants was probed by recording their intracellular Ca^{2+} signaling in response to stimulation with LTX^{N4C}, a mutant αLTX unable to form membrane pores (as described in Methods).[25,68–70] The wild-type (WT) ADGRL1 showed a large response to extracellular Ca^{2+} (Ca^{2+}_e) influx, followed by strong and persistent oscillatory calcium signaling in most cells. Similar to vector-transfected cells, cells expressing p.Trp9* did not react to LTX^{N4C} or native αLTX. Cells expressing p.Tyr346Cys demonstrated high influx of Ca^{2+}_e, but very few calcium oscillations. The Trp1005Arg construct only reacted to LTX^{N4C} by Ca^{2+}_e influx, without subsequent calcium waves. The two constructs with intracellular variants (p.Met1152Thr and p.Ser1164Phe) produced a low Ca^{2+}_e signal, followed by infrequent calcium oscillations in some cells. Thus, all ADGRL1 variants studied displayed impairments in LTX^{N4C}-induced intracellular calcium signaling (Figure 2D), indicating that they should be considered as pathogenic. Overall, our data indicate that the molecular consequences of ADGRL1 mutations are consistent with haploinsufficiency.

To model the pathophysiological effects of human *ADGRL1* haploinsufficiency, we inactivated *Adgrl1* in mice (described in Methods) (Figure S2A). When the colony was established, we noted a pronounced sub-Mendelian frequency of the *Adgrl1* null allele in the offspring and a lack of knockout (KO) progeny on the original 129/SvJ genetic background (Figure S2B), which suggested that the deletion of *Adgrl1* was embryonically lethal (for additional data see Supplemental Results, Figure S2). On this non-compensatory background, many heterozygous (HET) pups showed neurodevelopmental abnormalities. More than 15% of HET offspring were unable to move in a coordinated manner, failing to suckle or right themselves (Figure 3A, B). Some less affected HET animals that survived until weaning also demonstrated neurological deficits, e.g. seizures upon transfer to a new environment (Figure 3A). On this genetic background WT animals displayed no abnormalities (Figure 3B). For a more detailed description of behavioral data, see Supplemental Information.

After backcrossing to C57BL/6, some KO offspring were finally obtained, as demonstrated by polymerase chain reaction (PCR) and Western blotting for ADGRL1 protein (Figure S2C, D). Although proper Mendelian *Adgrl1*$^{-/-}$ frequency was still not achieved (Figure S2E), the C57BL/6 genetic background provided sufficient compensation of *Adgrl1* deletion for some KO animals to survive gestation (see also Supplemental Results, Figure S2F, G). On this more permissive genetic background, HET animals developed normally and revealed no behavioral or neurological deviations.

By contrast, most KO animals successfully completing their development demonstrated a host of aberrant behaviors. The main abnormality was persistent maternal infanticide. Thus, 71% of KO mothers killed their newborn pups (Figure 3C). The dead neonates never showed milk spots, indicating a lack of nursing, but the promptness of the attack (usually within minutes postpartum) and its exhaustive character (all pups killed) suggested a deliberate act of aggression due to an affective dysfunction rather than litter abandonment, passive cannibalism or inability to bond. The KO dams showed no adaptation to litters' demands with consecutive parturitions (Figure 3D), which indicates also some cognitive dysfunction.

KO male mice also frequently killed their offspring, however, they did it ~2.5 times less frequently than KO dams (Figure 3C). Similar to KO females, KO males showed no adaptation to periodic appearances of litters, killing the same percent of litters after each parturition taking place in their home cage (Figure 3D). The fact of paternal infanticide argued against postpartum psychosis as the main reason of maternal infanticide, but was consistent with faulty sensory gating in KO animals. When both parents lacked *Adgrl1*, they always killed their offspring (Figure 3C, D). Importantly, WT-HET and WT-WT pairs on the compensatory genetic background never killed their offspring, while only one HET-HET pair ever committed infanticide (1 out of 31).

KO animals also demonstrated aberrant social and sexual interactions. Thus, 50% of matings involving at least one KO animal remained nulliparous, while only 20% of WT/HET breeding pairs produced no progeny (Figure 3E). Although many reasons could underlie sexual dysfunction, we noted that the KO animals demonstrated a bimodal distribution. While some KO mice conceived/sired repeatedly, albeit regularly killing their pups, other animals were consistently averse to reproductive behavior. These two modalities suggested the presence of either a bipolar affective disorder or a bimodal cognitive impairment, such as schizophrenia.

To begin distinguishing between these possibilities, we studied locomotor activity in the *Adgrl1*$^{-/-}$ mice. Given their exaggerated response to novel stressful stimuli, we initially assessed their routine behavior using home-cage running wheels. As shown in Figure 3F, KO mice often demonstrated hyperactive behavior, greatly exceeding their WT or HET littermates in locomotion. Intriguingly, the KO animals fell into two opposite categories: either strongly hyperactive or strongly hypoactive (Figure 3G), which resembled manic and depressive states. WT and HET mice showed much less variance in these tests (Figure 3G). However, we did not observe any spontaneous switching between the two polar behavioral types, which may suggest that the KO animals had either one disorder with two invariable modalities or a spectrum of separate disorders.

Stress response and extremes of locomotion in the KO mice were consistent with impaired sensorimotor gating, therefore, we tested them in acoustic startle and pre-pulse inhibition (PPI) experiments, designed to assess animals' attention and sensory gating deficits in relation to salient environmental stimuli.[63,73] The KO mice demonstrated a clearly increased startle response (Figure 3H, NS protocol; Figure 3I). When the startle stimulus was shortly preceded by a sub-threshold acoustic pre-pulse (PS protocol) (Figure 3H), the startle response was inhibited by 40% in WT mice, but only by 10% in KO mice (Figure 3I, J). To assess the involvement of monoaminergic neurotransmission in the startle responses observed, we injected WT and KO mice with 1 mg/kg risperidone, an atypical antipsychotic and an antagonist at dopamine and 5-HT receptors. This increased the PPI to ~60% for WT and to ~45% for KO mice (Figure 3I, J), while also attenuating the difference between these cohorts. These results confirm the abnormal sensorimotor gating in *Adgrl1*$^{-/-}$ mice and suggest an involvement of dopaminergic and/or serotonergic receptors.

Finally, the HET animals on the non-compensatory background and the KO mice on the compensatory genotype displayed persistent stereotypic behaviors: compulsive grooming, repetitive serial movements, excessive digging, tonic immobility etc., especially when transferred into a new cage. As an example, self-grooming in a new environment was twice longer, or more frequent, in KO mice than WT animals (Figure 3K). For additional results of behavioral tests, see Supplemental Information. These behaviors are similar to those of mutant mice with neuropsychiatric dysfunctions or increased release of dopamine in the brain.[74,75]

We then investigated the molecular and synaptic characteristics of the *Adgrl1* KO mice. The amount of ADGRL1 protein expressed in the brain of these mice corresponded well to the dose of the *Adgrl1* allele (Figure 4A, B). These changes in ADGRL1 protein affected the expression of other related proteins, in particular, the ADGRL1 paralogs, ADGRL2 and ADGRL3, and the ADGRL1 ligand, TEN2(or LASSO).[27,30] Specifically, the amounts of ADGRL2 and TEN2 in KO brains were, respectively, 12% and 19% lower than those in WT brains (Figure 4A and B). In contrast to these moderate changes, the expression of the more distant paralog ADGRL3 was dramatically affected (Figure 4A, B): HET and KO brains contained, respectively, 20% and 60% less ADGRL3 than WT brains. These data indicate that not only TEN2, which directly interacts with ADGRL1, but also ADGRL3 display coordinated expression with ADGRL1 and thus may interact with it physically, functionally or both.[30,31]

ADGRL1 has been hypothesized to regulate the activity of both central and peripheral synapses.[30,67,76]

Therefore, we studied spontaneous release of acetylcholine, glutamate and dopamine in KO mice. Surprisingly, KO mice displayed an increased basal release of these neurotransmitters (Figure 4C, D). Thus, spontaneous miniature end-plate potentials (mEPPs) were 2.5 times more frequent at KO neuromuscular junctions (NMJs) than at WT NMJs. This effect was purely presynaptic, because the mEPPs amplitude was unchanged (Figure S2H). Likewise, the release of glutamate and dopamine from isolated synaptic terminals (synaptosomes) prepared from KO mouse brains was significantly ameliorated compared to WT mouse synaptosomes (Figure 4D). Although unexpected, the increased neurotransmitter release in KO mice was consistent with their hyperactivity and dysfunctional sensorimotor gating.

Given that ADGRL1 was identified as the major Ca^{2+}-independent receptor for αLTX,[23,25,60] we tested whether ADGRL1 ablation led to any changes in αLTX binding and activity. Indeed, the disruption of the *Adgrl1* allele clearly decreased toxin binding (Figure 4E). However, about 30% of Ca^{2+}-independent αLTX binding still remained in the KO brains. To determine whether this residual binding could be responsible for any effects of αLTX, we treated cerebrocortical synaptosomes and NMJs from the *Adgrl1*$^{-/-}$ mice with LTX^{N4C}.[25,67,77,78] This toxin strongly stimulated spontaneous exocytosis of glutamate from WT synaptosomes (Figure 4F) and acetylcholine from WT and HET NMJs (Figure 4G), while only affecting mEPPs frequency, but not the amplitudes (Figure S2I), and thus acting purely presynaptically. By contrast, despite substantial toxin binding (Figure 4E and data not shown), KO synaptosomes and NMJs did not react to LTX^{N4C} (Figure 4F, G). These results demonstrate that ADGRL1 is indeed the main mediator of the receptor-dependent effects of LTX^{N4C} and that any changes in KO mouse brain functions most likely reflect ADGRL1 removal.

Combined, the above data suggested dysfunctional neuronal transmission at least in some KO synapses. To study synaptic transmission in central synapses in more detail, we prepared dissociated neuronal cultures from the hippocampi of WT and KO neonates. Using whole-cell patch-clamp recordings we simultaneously recorded spontaneous activity of excitatory and inhibitory synapses formed by hippocampal neurons in culture (Figure 4H). The features of both excitatory and inhibitory miniature postsynaptic currents (mEPSCs and mIPSCs, respectively) were very similar in WT and KO mice, including their shapes and amplitudes (Figure 4I; Figure S2J). However, synapses formed by KO neurons *in vitro* showed a much lower frequency of spontaneous firing than WT neurons: the mIPSC frequency was ~4 times lower and the mEPSC frequency 83-fold lower in KO cultures than in WT cultures (Figure 4H, J).

This dramatic loss of spontaneous synaptic activity in cultured KO neurons was in stark contrast to an increased spontaneous synaptic activity in *ex vivo* synapses. We hypothesized that KO neurons form synapses *in vitro* much less efficiently than WT neurons, and this results in a lower recorded activity. This hypothesis was tested by immunostaining KO and WT neuronal cultures with antibodies against vesicular transporters of glutamate (VGLUT) and γ-aminobutyric acid, GABA (VGAT). As demonstrated in Figure 4K, L, inhibitory synapses (identified by the anti-VGAT antibody) were much less numerous in KO neuronal cultures than in WT cultures. Likewise, and in agreement with the recorded synaptic activity, excitatory synapses (identified by the anti-VGLUT antibody) were exceptionally rare in KO neuron cultures compared to WT cultures. Thus, the decreased synaptic activity in KO hippocampal cultures was most probably caused by poor synapse formation (or survival) in cultured KO neurons.

In summary, the lack of ADGRL1 significantly enhances basal spontaneous synaptic activity in cholinergic, glutamatergic and dopaminergic synapses, but blocks $\mathrm{LTX}^{\mathrm{N4C}}$-induced neurotransmitter release *in vivo*, while decreasing the rate of synapse formation *in vitro*.

Discussion

Previous molecular and physiological studies using mammalian models have demonstrated preferential brain expression of ADGRL1 protein and suggested that it plays an important role in neuronal functions and maturation during early brain development and adult life. However, very few studies have addressed *ADGRL1* in humans, it has never been directly implicated in human pathology and its role remains poorly defined. Here, we first describe a cohort of individuals presenting with a neurodevelopmental disorder and carrying pathogenic heterozygous variants in *ADGRL1*. Furthermore, our results also show an important correlation between the disruption of *Adgrl1* in KO mice and a neurodevelopmental phenotype.

We show here that on two distinct genetic backgrounds, the deletion of this gene is either lethal or partially lethal, leading to a sub-Mendelian ratio of the null allele in offspring genotypes (Figure S2B, E). This was unexpected, because a previous more limited study did not report another *Adgrl1*$^{-/-}$ mouse line to deviate from Mendelian genotype distribution.[41] However, our extensive breeding data indicate that, on a compensatory background, the disruption of the *Adgrl1* allele causes ~50% lethality of KO embryos (Figure S2E). Those KO animals that survive gestation generally develop normally, but demonstrate profound behavioral abnormalities.

The most obvious phenotype in *Adgrl1* KO animals was frequent, deliberate parental neonaticide (Figure 3C). One factor known to cause aggression in mice is the maintenance conditions.[79–81] However, the neonaticide was committed by KO parents only; the colony was maintained in a standard rodent facility; and the conditions were explicitly altered several times during the study, which had no effect on the frequency of infanticide. The specific circumstances of this behavior suggest that KO mice were in a state of hypervigilance/over-arousal, and when the major disturbance of parturition occurred, mother’s sensory endurance was overloaded by physical demands from the pups, leading her to experience intense distress in the presence of the feared stimulus (her own litter). This indicates a failure to respond properly to environmental intrusions, i.e. a dysfunction of sensory processing.

Similarly, KO males also frequently killed their offspring, but demonstrated extreme aggression more rarely than KO females for several possible reasons: (1) only some of the pups’ demands affected the fathers, thus rarely exceeding their sensory threshold; (2) the WT/HET females that were usually paired with KO males always nurtured their pups and possibly protected them; (3) the normal maternal behavior of the WT/HET females could have a calming effect on the distressed KO males. The stochastic nature of the infanticide suggested a consistent, but not completely penetrant, behavioral pattern in both female and male KO mice that could be attenuated by unknown factors, occasionally allowing the parents to spare and rear some of their litters. On the other hand, a lack of habituation to the repeated appearance of an offspring (Figure 3D) indicated the presence of general cognitive/learning deficits.

Faulty sensorimotor gating in the *Adgrl1* KO mice was directly confirmed in the acoustic startle response and PPI experiments (Figure 3H-J). PPI is predominantly used to probe gating deficits in schizophrenia,[63] and the PPI in our *Adgrl1*$^{-/-}$ mice responded to the antipsychotic drug risperidone (Figure 3I, J), implicating dopaminergic and/or serotonergic brain circuits in this phenotype. Indeed, direct measurements demonstrated a significantly upregulated release of dopamine in prefrontal cortices of *Adgrl1*$^{-/-}$ mice (Figure 4D). Furthermore, ADGRL1 protein has been implicated in fine regulation of neurotransmitter release, while *Adgrl1* has been indirectly linked to schizophrenia.[45,82] On the other hand, bipolar disorder individuals also demonstrate a reduced PPI,[83] and this is consistent with the bimodal pattern of locomotor activity in our *Adgrl1*$^{-/-}$ mice (Figure 3F, G) and the two modalities of behavior observed in their infanticide chronology (Figure 3D). Thus, in our study, the PPI test most likely detected a variable spectrum of neurological conditions, similar to those found in humans with variants in *ADGRL1*.

The sensory overload and locomotor hyperactivity in *Adgrl1* KO mice appeared to correlate with strongly increased spontaneous release of glutamate and dopamine in their prefrontal brain areas, and of acetylcholine at their NMJs (Figure 4C, D). As the activation of ADGRL1 protein by LTX^{N4C}, TEN2 or A1 ScFv antibody is known to cause massive increase in spontaneous synaptic activity, this aGPCR has been hypothesized to regulate neurotransmitter release at presynaptic nerve terminals.[30,39,84] Therefore, it was initially unclear why ADGRL1 deletion caused an increase (rather than a decrease) in unstimulated release of glutamate, dopamine, and acetylcholine in KO mice. However, both central and peripheral KO synapses were insensitive to LTX^{N4C} (Figure 4E-G), which demonstrates the role for ADGRL1 in controlling synaptic activity and suggests that KO synapses, not activated via ADGRL1, have developed a mechanism of increased spontaneous transmitter secretion to compensate for ADGRL1 absence.

ADGRL1 deletion also led to impaired synapse formation in neuronal cultures, where it affected excitatory synapses more profoundly (Figure 4H-L). This is in line with the previous observation that ADGRL2 and 3 may be involved in specifying the pattern of excitatory synapse formation *in vitro*, which depends on simultaneous binding of two ADGRL1 ligands, TEN2 and FLRT3.[85] On the other hand, ADGRL1 deletion also caused dramatic ADGRL3 hypomorphism (Figure 4A, B). Thus, some of the phenotypical manifestations of ADGRL1 deletion could be due to the lower expression of ADGRL3 rather than the lack of ADGRL1. Indeed, mutations in *ADGRL3* have been linked to ADHD in humans.[45,50] However, the previous studies did not look at the possibility that mutations in *ADGRL3* could cause *ADGRL1* hypomorphism, an effect reciprocal to that described here for the *Adgrl1*$^{-/-}$ mice. Our observations suggest that the molecular basis of any neurodevelopmental disorders caused by mutations in *ADGRL1* or *ADGRL3* in humans may be complex, involving not only both these proteins, but also their interacting partners (TEN2, FLRT3).

One interesting question from our study is which genetic change/s could mitigate the embryonic lethality caused by *Adgrl1* inactivation in mice? This question requires further in-depth studies, but one likely candidate is the already mentioned hypomorphic *Adgrl3* allele, which was a serendipitous consequence of extensive breeding and selection for an *Adgrl1*$^{-/-}$-permissive background. The resultant decrease in ADGRL3 expression could indeed represent such a compensatory response, offsetting the absence of ADGRL1. If ADGRL1 and ADGRL3 are interdependent and physiologically antagonistic, their functions would normally remain in balance, but a loss of one protein would lead to an unabated activity of the other and thus jeopardize animals' development/viability. Interestingly, the lack of ADGRL1 in mouse brain did not lead to any appreciable changes in the expression of NRXN1, suggesting that these two αLTX receptors are probably not functionally connected.

As shown above, the behavioral phenotypes of mice lacking ADGRL1, in many aspects, resembled those that are displayed by humans with pathogenic variants in *ADGRL1*. Neuropsychiatric and cognitive phenotypes in mice do not always perfectly match human behaviors and are not easy to interpret, however, it is clear from these data that the loss of ADGRL1 expression in mice is responsible for a broad neurodevelopmental phenotype. This provides a strong argument for extrapolating these data to humans.

The occurrence of variants in *ADGRL1* in 10 individuals from 9 unrelated families with overlapping neurodevelopmental and neurological phenotypes, corroborated by the functional studies, strongly implicates *ADGRL1* variants in intellectual disability and developmental delay. We could not identify any genotype-phenotype correlations. Emblematically, individuals 3 and 4 (F3-II-5 and F3-II-6 respectively) from the same family showed a variable expressivity of the symptoms associated with the same variant (Figure 1B). Among the most interesting variants identified are the p.Trp9* and p.Trp278* nonsense variants, which would be expected to result in a lack of the full-size ADGRL1 protein. Indeed, our *in vitro* data indicate that at least the p.Trp9* mutant does not express any ADGRL1 protein (Figure 2A). Intriguingly, 5 out of 8 individuals including I3 and I5 (with the p.Trp278* and p.Trp9* variant, F3-II-5 and F4-II-1 respectively) demonstrate ASD/ADHD symptoms (Figure 1B), indicating that the lack of *ADGRL1* expression could be directly associated with ADHD. This is further corroborated by the fact that several unrelated individuals, lacking different segments of chromosome 19p that include *ADGRL1*, also present with hyperactivity and intellectual disability.[42] In addition, mutations that affect the ADGRL1 function in humans (p.Trp1005Arg and p.Ser1164Phe) (Figure 2C, D) also lead to ASD/ADHD symptoms (Figure 1B). Finally, the *Adgrl1*$^{-/-}$ mice described above demonstrate hyperactivity and cognitive deficits, consistent with human phenotypes.

Thus, while the effect of individual *ADGRL1* variants will have to be studied further in detail, we can already conclude that perturbations in ADGRL1 functions or its deletion seem to be associated mainly with cardinal symptoms including developmental delay with delayed speech development, intellectual disability, ASD, ADHD and, less frequently, epilepsy. However, these symptoms appear to be of variable expressivity, in line with our model studies in *Adgrl1* KO mice, where the *Adgrl1*$^{-/-}$ phenotype strongly depended on the genetic background. In addition, several other inconstant features were identified in our work, such as nonspecific facial dysmorphism, macrocephaly, generalized hypotonia, joint hypermobility, dermatological issues, genital anomalies or delayed puberty. It would be premature to conclude on any association between these secondary features and the *ADGRL1* variants based on a single human cohort, although due to the significant expression of *ADGRL1* in multiple tissues, these symptoms could be part of the *ADGRL1*-associated phenotype.

In conclusion, we provide a first overview of the phenotypes associated with *ADGRL1* variants in humans. These phenotypes are strongly supported by the data from *Adgrl1*$^{-/-}$ mice. Additional functional studies and identification of a larger cohort of individuals carrying pathogenic *ADGRL1* variants through international data sharing will be necessary to clarify the phenotypic spectrum associated with this gene and its counterpart, *ADGRL3*. We hope this information will help to achieve a better interpretation of any new *ADGRL1* variants that may be identified after exome/genome sequencing, leading to a better understanding and diagnosis of individuals with neurodevelopmental disorders.

Declaration of interests

The Department of Molecular and Human Genetics at Baylor College of Medicine receives revenue from clinical genetic testing completed at Baylor Genetics Laboratories. AC is an employee of GeneDx, Inc.

Acknowledgements

We thank the individuals and their families for their participation. We thank the Integragen society and CNG for exome analysis in some cases. We thank Evan E. Eichler and his laboratory for sharing clinical data of individual 5. This work was supported by grants from the Regional Council of Burgundy (PARI) and the FEDER. This work was also in part supported by a Wellcome Trust Project Grants GR074359MA and WT083199MF, Biotechnology and Biological Science Research Council Core Support Grants BBD523078 and BBF0083091, and core funding from the University of Kent School of Pharmacy (to Y.A.U.).

Data and code availability

The published article includes all data generated or analyzed during the study.

Publicly available data utilized in this work were obtained from NHLBI GO Exome Sequencing Project (see URLs) and its ongoing studies which produced and provided exome variant calls for comparison: the Lung GO Sequencing Project (HL-102923), the WHI Sequencing Project (HL-102924), the Broad GO Sequencing Project (HL-102925), the Seattle GO Sequencing Project (HL-102926), the Heart GO Sequencing Project (HL-103010) and the Rare Disease Initiative Zürich (RADIZ), Clinical Research Priority Program for Rare Diseases of the University of Zurich.

Web resources

https://esp.gs.washington.edu/drupal

https://gnomad.broadinstitute.org

https://www.proteinatlas.org

https://stuart.radboudumc.nl/metadome

Figure 1. Individuals and variants identified in our cohort. A, Schematic representation of ADGRL1 protein and distribution of the pathogenic variants reported in the study. Galactose binding lectin domain (GL), olfactomedin-like domain (OLF), hormone receptor domain (HRM), GPCR-autoproteolysis inducing domain (GAIN), GPCR proteolysis site domain (GPS), 7 transmembrane domain (7TM) and cytosolic latrophilin domain are depicted. Nonsense and frameshift variants are indicated in red. Missense variants are indicated in black. **B,** Variant segregation analysis in the families described in this cohort. Individuals with documented evaluation are indicated as i1-i10. Arrows indicate the first family member coming to medical attention. E_1 indicates exome results regarding *ADGRL1*. E_2 refers to the pathogenic *TAOK1* variant (p.Trp188*) identified in family F9 (Table 1). DD, developmental delay; ID, intellectual disability; ASD, autism spectrum disorder; ADHD, attention deficit hyperactivity disorder. **C,** Individuals with pathogenic *ADGRL1* variants.

Figure 2. *In vitro* analysis of mutations in human *ADGRL1*. A, Expression and surface delivery of the mutated constructs in NB2a cells. Cells transfected with the vector expressing WT ADGRL1, its variants (as indicated) or no ADGRL1 (Vector) were incubated with αLTX, lysed and immunoblotted with antibodies against the NTF of ADGRL1, αLTX and β-actin. In a separate experiment, surface exposure of p.M1152T and p.S1164F was detected by biotinylation of live cells and staining of the lysate with streptavidin. The blots represent n = 3 experiments, with similar results. M, molecular mass markers. **B**, Quantification of surface expression of the ADGRL1 mutants relative to native ADGRL1 (n = 3). **C**, Cytosolic calcium signaling induced in individual NB2a cells transfected with *ADGRL1*, its variants or an empty vector, and detected using confocal microscopy and an intracellular fluorescent Ca^{2+} sensor, Fluo-4. As indicated by arrowheads, the cells were first stimulated by buffer or 2 nM LTX^{N4C} in the absence of extracellular calcium, then 2 mM Ca^{2+}_e was added, and at the end of the procedure cells were treated with 1 nM αLTX, to form membrane pores and detect maximal fluorescence. Two exemplary traces are shown for each variant; the number of cells analyzed was 72-93, in n = 3-7 independent experiments. **D**, Quantification of integrated calcium signals in the cells expressing ADGRL1 or its mutants.

Figure 3. Cognitive and behavioral abnormalities in *Adgrl1*$^{-/-}$ mice. A-B, Neurological deficits in the offspring on the mixed 129/SvJ-C57BL/6 background. **A, Left**, An example of a loss of righting reflex in a P4 HET pup, compared to its WT littermate. **Centre**, A P3 HET pup underdeveloped due to suckling problems, with its WT littermate. **Right**, An example of a P21 HET pup experiencing arrest and seizures after transfer into a new environment (open space). **B**, The frequency of neurodevelopmental deficits in WT, HET and KO pups (circles, mean values; bars, ± 95% confidence intervals, CI; whiskers, ± 99% CI's. WT, n = 23; HET, n = 28 normal, 6 compromised; KO, n = 1 normal, *estimated* 23 dead in utero). **C-J**, Behavioral abnormalities in the *Adgrl1*$^{-/-}$ colony on the compensatory C57BL/6 background. **C**, Per cent of breeding pairs of specified genotype committing parental infanticide (X = WT or HET; circles, mean values; bars, ± 95% CI's; whiskers, ± 99% CI's). **D**, Consecutive litters killed by parents of indicated genotype. **E**, Parity in breeding pairs of specified genotypes (X = WT or HET; circles, mean values; bars, ± 95% CI; all KO pairs n = 156, nulliparous n = 72; all WT pairs n = 20, nulliparous n = 4). **F**, Examples of running wheel activity of WT and KO littermates (ticks correspond to revolutions per min). **G**, Average wheel-running activity in mice of indicated genotypes (KO animals are plotted as two groups of high or low locomotor activity; WT or

HET, n = 8; KO, n = 4 and 4). **H**, Typical auditory startle reflex responses in WT and KO mice under indicated protocols (respective individual traces overlaid). Trial types: PN, pre-pulse, no startle stimulus; NS, no pre-pulse, startle stimulus; PS, pre-pulse, startle stimulus; RIS, 1 mg/kg risperidone, 30 min prior to test. (WT animals, n = 6 vehicle group, n = 4 risperidone group; KO animals, n = 4 vehicle group, n = 4 risperidone group). **I**, Quantification of startle responses as in H. **J**, PPI in PS trials in control and risperidone-treated animals. **K**, Overall time spent self-grooming by WT and KO mice over a 10-min period in a new environment. (WT animals, n = 9; KO animals, n = 10).

Figure 4. Protein expression, synaptic activity and synapse formation in *Adgrl1*$^{-/-}$ mice. A, Expression of the ADGRL family proteins and TEN2 in WT, HET and KO mouse brains. A representative Western blot of brain membranes, stained for the NTFs of ADGRL proteins and the C-terminal fragment of TEN2. β-Actin was used to control gel loading. **B**, Quantification of receptor expression, as in E (ADGRL1, n = 5; ADGRL2, n = 5-9; ADGRL3, n = 5-6; TEN2, n = 3-5; NRXN1, n = 3-6). **C**, Increased spontaneous release of acetylcholine (electrophysiologically recorded as mEPPs) at KO mouse NMJs. Left, Representative raw traces; right, quantification of mEPPs frequency at WT and KO mouse NMJs (p < 0.012; WT, n = 8; KO, n = 11). **D**, Increased release of glutamate (Glu) and dopamine (DA) from synaptosomes isolated from KO mouse brain. Synaptosomes were preloaded with [^{14}C]Glu and [^{3}H]DA and incubated for 15 min without stimulation (Glu release, p < 0.0008, n = 6; DA release, p < 0.0041, n = 6). NT, neurotransmitter. **E**, Specific Ca^{2+}-independent binding of ^{125}I-LTX to cerebrocortical synaptosomes from the WT and KO mice (n = 6). **F**, LTX^{N4C} (1 nM) increases glutamate release from the WT, but not KO, synaptosomes in the presence of 2 mM Ca^{2+} (n = 6). **G**, LTX^{N4C} increases the mEPPs frequency at the NMJs of WT and HET mice, but not KO mice. Left, representative original recordings; right, frequencies of LTX^{N4C}-evoked mEPPs (WT, n = 6; HET, n = 3; KO, n = 5 independent animals). **H**, Spontaneous synaptic activity is greatly decreased in KO hippocampal cultures. Patch-clamp recordings demonstrate a regular occurrence of both mIPSCs (upward spikes) and mEPSCs (downward spikes) in WT hippocampal cultures, and a much rarer detection of mIPSCs and especially mEPSCs in KO cultures. **I**, The amplitudes and shapes of average miniature postsynaptic currents are similar in hippocampal cultures from WT and KO mice. **J**, The frequencies of mIPSCs and mEPSCs in WT and KO neuronal cultures (n = 28 cells from 6 experiments for each condition). **K**, KO neurons in culture form a lower number of inhibitory and especially excitatory synapses compared to WT neurons. Hippocampal cultures from P1 WT and KO brains were grown for 21 days and stained with antibodies against VGAT (inhibitory synapses) or VGLUT (excitatory synapses). The images are representative of n = 5 experiments. **L**, Quantification of inhibitory and excitatory synapse formation in WT and KO hippocampal cultures (n = 5 for both conditions).

Table 1. Clinical features and variants found in the 9 individuals of the cohort

	Individual 1	Individual 2	Individual 3[a]	Individual 4[a]	Individual 5 (Guo et al., 2019)[57]	Individual 6	Individual 7	Individual 8	Individual 9	Individual 10
Sex	Male	Male	Female	Female	Male	Male	Female	Male	Male	Male
Age at last examination	11y[b]	3y 3mth[c]	12y 1mth	11 y 1mth	19y	10y	13y	10y	8y	43y
Birth measurements										
Weight in g (centile)	3780 (83th)	NA[d]	2950 (14th)	3720 (87th)	NA	NA	3000 (2-9th)	4470 (>97th)	4100(90th)	NA
Length in cm (centile)	53 (95th)	NA	50 (55th)	52 (94th)	NA	NA	54 (50-75th)	57 (>97th)	51(75th)	NA
OFC[e] in cm (centile)	39 (99th)	NA	34,5 (52th)	37 (98th)	NA	NA	NA	NA	36,5(75th)	NA
Developmental features										
Age at sitting (months)	18	delayed	12	7	NA	NA	NA	7	9	12
Age at walking (months)	23	delayed	13	14	NA	17	11	30	16	17
Age at first words (months)	15	delayed	24	12	NA	24	14	36	36	15
Developmental delay	+	+	+	+	-	+	+	+	+	+
Intellectual disability degree (IQ)[g]	mild to moderate	NA	mild	mild (IQ 57)	IQ 96	no ID[f]	borderline (IQ 74)	IQ 109	mild to moderate	mild
ASD[h]	+	NA	+	-	+	-	-	+	-	-
ADHD[i]	+	NA	+	-	suspected	-	+	-	-	-
Neurological features										
Hypotonia	+	NA	+	+	-	-	-	+	-	-
Stereotypies	+	NA	-	-	-	-	NA	+	-	-
Epilepsy	-	NA	-	-	-	-	+	+	-	-
Sleep disturbance	+	NA	+	+	-	+	+	-	-	-
Brain imaging	normal	NA	NA	NA	NA	nodular heterotopia	normal	normal	normal	NA
Facial dysmorphism	-	+[j]	-	+	-	+	+	+	+	+
Additional features										

Macrocephaly	congenital	NA	Postnatal (93thcentile)	+	NA	-	NA	NA	+ (97thcentile)	-
Overweight	-	NA	+ (99th centile)	+	+	-	-	-	-	+
Joint hypermobility	+	NA	+	-	-	+	NA	+	-	-
Others	Hyperopia Temporary regression Megadolichocolon	Learning disabilities	Hyperkinetic disorder Small hands and feet	Small hands and feet	Poor adaptive skills Learning disabilities	Migraine Dermatological issues Genital abnormalities Borderline short stature Advance bone age Clinodactyly	Delayed puberty	Dermatological issues Scoliosis	Learning disabilities	2 Neuroendocrine pancreatic tumors at 43y
ADGRL1 variant DNA change GRCh37/hg19 NC_000019.9 (chr19)	g.14267505A>G	g.14263628G>A	g.14273794C>T	g.14273794C>T	g.14294389C>T	g.14263409A>G	g.14263373G>A	g.14270002dup	g.14263332G>A	g.14273591T>C
cDNA **change** NM_001008701.2	c.3013T>C	c.3406C>T	c.834G>A	c.834G>A	c.26G>A	c.3455T>C	c.3491C>T	c.2064dup	c.3532C>T	c.1037A>G
Amino acid chance	p.Trp1005Arg	p.Arg1136*	p.Trp278*	p.Trp278*	p.Trp9*	p.Met1152Thr	p.Ser1164Phe	p.Glu689Argfs*113	p.Arg1178*	p.Tyr346Cys
Inheritance	*de novo*	*de novo*	paternally inherited	paternally inherited	*de novo*	*de novo*	*de novo*	*de novo*	*de novo*	*paternally inherited*
Additional findings:	-	*9p13.3 Deletion*	-	-	-	*5q14.3 Deletion*	-	-	*6p12.3 Duplication*	*TAOK1*
Variant GRCh37/hg19		*(34655686-34662203) x1*				*(83112653-85261932)x1*			*(47075799-48930453)x3*	*NM_020791.1: c.564G>A*
Amino acid change										p.Trp188*
OMIM Gene Phenotypes		*IL11RA* Craniosynostosis and dental anomalies AR[k] MIM 614188				-			*CD2AP* Glomerulosclerosis, focal segmental 3 MIM 607832	Developmental delay with or without intellectual impairment or behavioral abnormalities AD[l] MIM 619575
ACMG[m] classification		*VUS*[n]				*VUS*			*VUS*	*pathogenic*

Inheritance	*unknown*				*maternally inherited*			*maternally inherited*	*paternally inherited*

[a] siblings
[b] years
[c] months
[d] not available
[e] occipital frontal circumference
[f] intellectual disability
[g] intellectual quotient
[h] **autism spectrum disorder**
[i] attention-deficit hyperactivity disorder

[j] probably not linked to *ADGRL1* variant;
[k] autosomal recessive
[l] autosomal dominant
[m] American College of Medical Genetics and Genomics classification
[n] variant of unknown significance

Reference

1. Hauser, A.S., Attwood, M.M., Rask-Andersen, M., Schiöth, H.B., and Gloriam, D.E. (2017). Trends in GPCR drug discovery: new agents, targets and indications. Nat Rev Drug Discov *16*, 829–842.

2. Grammatopoulos, D.K. (2017). Regulation of G-protein coupled receptor signalling underpinning neurobiology of mood disorders and depression. Molecular and Cellular Endocrinology *449*, 82–89.

3. Leung, C., and Wong, Y. (2017). Role of G Protein-Coupled Receptors in the Regulation of Structural Plasticity and Cognitive Function. Molecules *22*, 1239.

4. Kooistra, A.J., Mordalski, S., Pándy-Szekeres, G., Esguerra, M., Mamyrbekov, A., Munk, C., Keserű, G.M., and Gloriam, D.E. (2021). GPCRdb in 2021: integrating GPCR sequence, structure and function. Nucleic Acids Research *49*, D335–D343.

5. Byrne, K.F., Pal, A., Curtin, J.F., Stephens, J.C., and Kinsella, G.K. (2021). G-protein-coupled receptors as therapeutic targets for glioblastoma. Drug Discovery Today S1359644621003159.

6. Bae, B.-I., Tietjen, I., Atabay, K.D., Evrony, G.D., Johnson, M.B., Asare, E., Wang, P.P., Murayama, A.Y., Im, K., Lisgo, S.N., et al. (2014). Evolutionarily Dynamic Alternative Splicing of GPR56 Regulates Regional Cerebral Cortical Patterning. Science *343*, 764–768.

7. Piao, X., Hill, R.S., Bodell, A., Chang, B.S., Basel-Vanagaite, L., Straussberg, R., Dobyns, W.B., Qasrawi, B., Winter, R.M., Innes, A.M., et al. (2004). G Protein-Coupled Receptor-Dependent Development of Human Frontal Cortex. Science *303*, 2033–2036.

8. Nazarko, O., Kibrom, A., Winkler, J., Leon, K., Stoveken, H., Salzman, G., Merdas, K., Lu, Y., Narkhede, P., Tall, G., et al. (2018). A Comprehensive Mutagenesis Screen of the Adhesion GPCR Latrophilin-1/ADGRL1. IScience *3*, 264–278.

9. Kuhnert, F., Mancuso, M.R., Shamloo, A., Wang, H.-T., Choksi, V., Florek, M., Su, H., Fruttiger, M., Young, W.L., Heilshorn, S.C., et al. (2010). Essential Regulation of CNS Angiogenesis by the Orphan G Protein–Coupled Receptor GPR124. Science *330*, 985–989.

10. Chae, J., Kim, M.J., Goo, J.H., Collier, S., Gubb, D., Charlton, J., Adler, P.N., and Park, W.J. (1999). The Drosophila tissue polarity gene starry night encodes a member of the protocadherin family. Development *126*, 5421–5429.

11. Langenhan, T., Prömel, S., Mestek, L., Esmaeili, B., Waller-Evans, H., Hennig, C., Kohara, Y., Avery, L., Vakonakis, I., Schnabel, R., et al. (2009). Latrophilin Signaling Links Anterior-Posterior Tissue Polarity and Oriented Cell Divisions in the C. elegans Embryo. Developmental Cell *17*, 494–504.

12. Shima, Y., Kengaku, M., Hirano, T., Takeichi, M., and Uemura, T. (2004). Regulation of Dendritic Maintenance and Growth by a Mammalian 7-Pass Transmembrane Cadherin. Developmental Cell *7*, 205–216.

13. Usui, T., Shima, Y., Shimada, Y., Hirano, S., Burgess, R.W., Schwarz, T.L., Takeichi, M., and Uemura, T. (1999). Flamingo, a seven-pass transmembrane cadherin, regulates planar cell polarity under the control of Frizzled. Cell *98*, 585–595.

14. Bolliger, M.F., Martinelli, D.C., and Sudhof, T.C. (2011). The cell-adhesion G protein-coupled receptor BAI3 is a high-affinity receptor for C1q-like proteins. Proceedings of the National Academy of Sciences *108*, 2534–2539.

15. Monk, K.R., Naylor, S.G., Glenn, T.D., Mercurio, S., Perlin, J.R., Dominguez, C., Moens, C.B., and Talbot, W.S. (2009). A G Protein–Coupled Receptor Is Essential for Schwann Cells to Initiate Myelination. Science *325*, 1402–1405.

16. Hu, G.-M., Mai, T.-L., and Chen, C.-M. (2017). Visualizing the GPCR Network: Classification and Evolution. Sci Rep *7*, 15495.

17. Araç, D., Boucard, A.A., Bolliger, M.F., Nguyen, J., Soltis, S.M., Südhof, T.C., and Brunger, A.T. (2012). A novel evolutionarily conserved domain of cell-adhesion GPCRs mediates autoproteolysis: Cell-adhesion GPCRs mediates autoproteolysis. The EMBO Journal *31*, 1364–1378.

18. Rosa, M., Noel, T., Harris, M., and Ladds, G. (2021). Emerging roles of adhesion G protein-coupled receptors. Biochemical Society Transactions *49*, 1695–1709.

19. Langenhan, T., Aust, G., and Hamann, J. (2013). Sticky Signaling—Adhesion Class G Protein–Coupled Receptors Take the Stage. Sci. Signal. *6*,.

20. Krishnan, A., Nijmeijer, S., de Graaf, C., and Schiöth, H.B. (2016). Classification, Nomenclature, and Structural Aspects of Adhesion GPCRs. In Adhesion G Protein-Coupled Receptors, T. Langenhan, and T. Schöneberg, eds. (Cham: Springer International Publishing), pp. 15–41.

21. Dunn, H.A., Orlandi, C., and Martemyanov, K.A. (2019). Beyond the Ligand: Extracellular and Transcellular G Protein–Coupled Receptor Complexes in Physiology and Pharmacology. Pharmacol Rev *71*, 503–519.

22. Krasnoperov, V.G., Beavis, R., Chepurny, O.G., Little, A.R., Plotnikov, A.N., and Petrenko, A.G. (1996). The Calcium-Independent Receptor of α-Latrotoxin Is Not a Neurexin. Biochemical and Biophysical Research Communications *227*, 868–875.

23. Davletov, B.A., Shamotienko, O.G., Lelianova, V.G., Grishin, E.V., and Ushkaryov, Y.A. (1996). Isolation and Biochemical Characterization of a Ca2+-independent α-Latrotoxin-binding Protein. Journal of Biological Chemistry *271*, 23239–23245.

24. Krasnoperov, V.G., Bittner, M.A., Beavis, R., Kuang, Y., Salnikow, K.V., Chepurny, O.G., Little, A.R., Plotnikov, A.N., Wu, D., Holz, R.W., et al. (1997). α-Latrotoxin Stimulates Exocytosis by the Interaction with a Neuronal G-Protein-Coupled Receptor. Neuron *18*, 925–937.

25. Volynski, K.E., Capogna, M., Ashton, A.C., Thomson, D., Orlova, E.V., Manser, C.F., Ribchester, R.R., and Ushkaryov, Y.A. (2003). Mutant α-Latrotoxin (LTXN4C) Does Not Form Pores and Causes Secretion by Receptor Stimulation. Journal of Biological Chemistry *278*, 31058–31066.

26. Moreno-Salinas, A.L., Avila-Zozaya, M., Ugalde-Silva, P., Hernández-Guzmán, D.A., Missirlis, F., and Boucard, A.A. (2019). Latrophilins: A Neuro-Centric View of an Evolutionary Conserved Adhesion G Protein-Coupled Receptor Subfamily. Front. Neurosci. *13*, 700.

27. Matsushita, H., Lelianova, V.G., and Ushkaryov, Y.A. (1999). The latrophilin family: multiply spliced G protein-coupled receptors with differential tissue distribution. FEBS Letters *443*, 348–352.

28. Ichtchenko, K., Bittner, M.A., Krasnoperov, V., Little, A.R., Chepurny, O., Holz, R.W., and Petrenko, A.G. (1999). A Novel Ubiquitously Expressed α-Latrotoxin Receptor Is a Member of the CIRL Family of G-protein-coupled Receptors. Journal of Biological Chemistry *274*, 5491–5498.

29. Sugita, S., Ichtchenko, K., Khvotchev, M., and Südhof, T.C. (1998). α-Latrotoxin Receptor CIRL/Latrophilin 1 (CL1) Defines an Unusual Family of Ubiquitous G-protein-linked Receptors. Journal of Biological Chemistry *273*, 32715–32724.

30. Silva, J.-P., Lelianova, V.G., Ermolyuk, Y.S., Vysokov, N., Hitchen, P.G., Berninghausen, O., Rahman, M.A., Zangrandi, A., Fidalgo, S., Tonevitsky, A.G., et al. (2011). Latrophilin 1 and its endogenous ligand Lasso/teneurin-2 form a high-affinity transsynaptic receptor pair with signaling capabilities. Proceedings of the National Academy of Sciences *108*, 12113–12118.

31. Boucard, A.A., Maxeiner, S., and Südhof, T.C. (2014). Latrophilins Function as Heterophilic Cell-adhesion Molecules by Binding to Teneurins. Journal of Biological Chemistry *289*, 387–402.

32. Röthe, J., Thor, D., Winkler, J., Knierim, A.B., Binder, C., Huth, S., Kraft, R., Rothemund, S., Schöneberg, T., and Prömel, S. (2019). Involvement of the Adhesion GPCRs Latrophilins in the Regulation of Insulin Release. Cell Reports *26*, 1573-1584.e5.

33. Li, J., Xie, Y., Cornelius, S., Jiang, X., Sando, R., Kordon, S.P., Pan, M., Leon, K., Südhof, T.C., Zhao, M., et al. (2020). Alternative splicing controls teneurin-latrophilin interaction and synapse specificity by a shape-shifting mechanism. Nat Commun *11*, 2140.

34. Kreienkamp, H.-J., Zitzer, H., Gundelfinger, E.D., Richter, D., and Böckers, T.M. (2000). The Calcium-independent Receptor for α-Latrotoxin from Human and Rodent Brains Interacts with Members of the ProSAP/SSTRIP/Shank Family of Multidomain Proteins. Journal of Biological Chemistry *275*, 32387–32390.

35. Uchigashima, M., Cheung, A., Suh, J., Watanabe, M., and Futai, K. (2019). Differential expression of neurexin genes in the mouse brain. J Comp Neurol *527*, 1940–1965.

36. Boucard, A.A., Ko, J., and Südhof, T.C. (2012). High Affinity Neurexin Binding to Cell Adhesion G-protein-coupled Receptor CIRL1/Latrophilin-1 Produces an Intercellular Adhesion Complex. Journal of Biological Chemistry *287*, 9399–9413.

37. O'Sullivan, M.L., de Wit, J., Savas, J.N., Comoletti, D., Otto-Hitt, S., Yates, J.R., and Ghosh, A. (2012). FLRT Proteins Are Endogenous Latrophilin Ligands and Regulate Excitatory Synapse Development. Neuron *73*, 903–910.

38. Burbach, J.P.H., and Meijer, D.H. (2019). Latrophilin's Social Protein Network. Front. Neurosci. *13*, 643.

39. Vysokov, N.V., Silva, J.-P., Lelianova, V.G., Suckling, J., Cassidy, J., Blackburn, J.K., Yankova, N., Djamgoz, M.B., Kozlov, S.V., Tonevitsky, A.G., et al. (2018). Proteolytically released Lasso/teneurin-2 induces axonal attraction by interacting with latrophilin-1 on axonal growth cones. ELife *7*, e37935.

40. Jackson, V.A., del Toro, D., Carrasquero, M., Roversi, P., Harlos, K., Klein, R., and Seiradake, E. (2015). Structural Basis of Latrophilin-FLRT Interaction. Structure *23*, 774–781.

41. Tobaben, S., Südhof, T.C., and Stahl, B. (2002). Genetic Analysis of α-Latrotoxin Receptors Reveals Functional Interdependence of CIRL/Latrophilin 1 and Neurexin 1α. Journal of Biological Chemistry *277*, 6359–6365.

42. Bonaglia, M.C., Marelli, S., Novara, F., Commodaro, S., Borgatti, R., Minardo, G., Memo, L., Mangold, E., Beri, S., Zucca, C., et al. (2010). Genotype–phenotype relationship in three cases with overlapping 19p13.12 microdeletions. Eur J Hum Genet *18*, 1302–1309.

43. Li, Y.R., Li, J., Zhao, S.D., Bradfield, J.P., Mentch, F.D., Maggadottir, S.M., Hou, C., Abrams, D.J., Chang, D., Gao, F., et al. (2015). Meta-analysis of shared genetic architecture across ten pediatric autoimmune diseases. Nat Med *21*, 1018–1027.

44. Vezain, M., Lecuyer, M., Rubio, M., Dupé, V., Ratié, L., David, V., Pasquier, L., Odent, S., Coutant, S., Tournier, I., et al. (2018). A de novo variant in ADGRL2 suggests a novel mechanism underlying the previously undescribed association of extreme microcephaly with severely reduced sulcation and rhombencephalosynapsis. Acta Neuropathol Commun *6*, 109.

45. Arcos-Burgos, M., Jain, M., Acosta, M.T., Shively, S., Stanescu, H., Wallis, D., Domené, S., Vélez, J.I., Karkera, J.D., Balog, J., et al. (2010). A common variant of the latrophilin 3 gene, LPHN3, confers susceptibility to ADHD and predicts effectiveness of stimulant medication. Mol Psychiatry *15*, 1053–1066.

46. Ribasés, M., Ramos-Quiroga, J.A., Sánchez-Mora, C., Bosch, R., Richarte, V., Palomar, G., Gastaminza, X., Bielsa, A., Arcos-Burgos, M., Muenke, M., et al. (2011). Contribution of LPHN3 to the genetic susceptibility to ADHD in adulthood: a replication study. Genes, Brain and Behavior *10*, 149–157.

47. Acosta, M.T., Swanson, J., Stehli, A., Molina, B.S.G., the MTA Team, Martinez, A.F., Arcos-Burgos, M., and Muenke, M. (2016). *ADGRL 3 (LPHN 3)* variants are associated with a refined phenotype of ADHD in the MTA study. Mol Genet Genomic Med *4*, 540–547.

48. Bruxel, E.M., Moreira-Maia, C.R., Akutagava-Martins, G.C., Quinn, T.P., Klein, M., Franke, B., Ribasés, M., Rovira, P., Sánchez-Mora, C., Kappel, D.B., et al. (2021). Meta-analysis and systematic review of ADGRL3 (LPHN3) polymorphisms in ADHD susceptibility. Mol Psychiatry *26*, 2277–2285.

49. Domené, S., Stanescu, H., Wallis, D., Tinloy, B., Pineda, D.E., Kleta, R., Arcos-Burgos, M., Roessler, E., and Muenke, M. (2011). Screening of human LPHN3 for variants with a potential impact on ADHD susceptibility. Am. J. Med. Genet. *156*, 11–18.

50. Acosta, M.T., Vélez, J.I., Bustamante, M.L., Balog, J.Z., Arcos-Burgos, M., and Muenke, M. (2011). A two-locus genetic interaction between LPHN3 and 11q predicts ADHD severity and long-term outcome. Transl Psychiatry *1*, e17–e17.

51. Jain, M., Vélez, J.I., Acosta, M.T., Palacio, L.G., Balog, J., Roessler, E., Pineda, D., Londoño, A.C., Palacio, J.D., Arbelaez, A., et al. (2012). A cooperative interaction between LPHN3 and 11q doubles the risk for ADHD. Mol Psychiatry *17*, 741–747.

52. Labbe, A., Liu, A., Atherton, J., Gizenko, N., Fortier, M.-È., Sengupta, S.M., and Ridha, J. (2012). Refining psychiatric phenotypes for response to treatment: Contribution of LPHN3 in ADHD. Am. J. Med. Genet. *159B*, 776–785.

53. Fallgatter, A.J., Ehlis, A.-C., Dresler, T., Reif, A., Jacob, C.P., Arcos-Burgos, M., Muenke, M., and Lesch, K.-P. (2013). Influence of a Latrophilin 3 (LPHN3) risk haplotype on event-related potential measures of cognitive response control in attention-deficit hyperactivity disorder (ADHD). European Neuropsychopharmacology *23*, 458–468.

54. Martinez, A.F., Abe, Y., Hong, S., Molyneux, K., Yarnell, D., Löhr, H., Driever, W., Acosta, M.T., Arcos-Burgos, M., and Muenke, M. (2016). An Ultraconserved Brain-Specific Enhancer Within ADGRL3 (LPHN3) Underpins Attention-Deficit/Hyperactivity Disorder Susceptibility. Biological Psychiatry *80*, 943–954.

55. Field, L.L., Shumansky, K., Ryan, J., Truong, D., Swiergala, E., and Kaplan, B.J. (2013). Dense-map genome scan for dyslexia supports loci at 4q13, 16p12, 17q22; suggests novel locus at 7q36: High-density genome scan for dyslexia genes. Genes, Brain and Behavior *12*, 56–69.

56. Kappel, D.B., Schuch, J.B., Rovaris, D.L., da Silva, B.S., Müller, D., Breda, V., Teche, S.P., S. Riesgo, R., Schüler-Faccini, L., Rohde, L.A., et al. (2019). ADGRL3 rs6551665 as a Common Vulnerability Factor Underlying Attention-Deficit/Hyperactivity Disorder and Autism Spectrum Disorder. Neuromol Med *21*, 60–67.

57. Guo, H., Duyzend, M.H., Coe, B.P., Baker, C., Hoekzema, K., Gerdts, J., Turner, T.N., Zody, M.C., Beighley, J.S., Murali, S.C., et al. (2019). Genome sequencing identifies multiple deleterious variants in autism patients with more severe phenotypes. Genet Med *21*, 1611–1620.

58. Nambot, S., Thevenon, J., Kuentz, P., Duffourd, Y., Tisserant, E., Bruel, A.-L., Mosca-Boidron, A.-L., Masurel-Paulet, A., Lehalle, D., Jean-Marçais, N., et al. (2018). Clinical whole-exome sequencing for the diagnosis of rare disorders with congenital anomalies and/or intellectual disability: substantial interest of prospective annual reanalysis. Genet Med *20*, 645–654.

59. Berninghausen, O., Rahman, M.A., Silva, J.-P., Davletov, B., Hopkins, C., and Ushkaryov, Y.A. (2007). Neurexin Iβ and neuroligin are localized on opposite membranes in mature central synapses. J Neurochem *103*, 1855–1863.

60. Davletov, B.A., Meunier, F.A., Ashton, A.C., Matsushita, H., Hirst, W.D., Lelianova, V.G., Wilkin, G.P., Dolly, J.O., and Ushkaryov, Y.A. (1998). Vesicle exocytosis stimulated by α-latrotoxin is mediated by latrophilin and requires both external and stored Ca2+. EMBO J *17*, 3909–3920.

61. Volynski, K.E., Meunier, F.A., Lelianova, V.G., Dudina, E.E., Volkova, T.M., Rahman, M.A., Manser, C., Grishin, E.V., Dolly, J.O., Ashley, R.H., et al. (2000). Latrophilin, Neurexin, and Their Signaling-deficient Mutants Facilitate α-Latrotoxin Insertion into Membranes but Are Not Involved in Pore Formation. Journal of Biological Chemistry *275*, 41175–41183.

62. Davydov, I.I., Fidalgo, S., Khaustova, S.A., Lelyanova, V.G., Grebenyuk, E.S., Ushkaryov, Yu.A., and Tonevitsky, A.G. (2009). Prediction of Epitopes in Closely Related Proteins Using a New Algorithm. Bull Exp Biol Med *148*, 869–873.

63. Swerdlow, N.R., Weber, M., Qu, Y., Light, G.A., and Braff, D.L. (2008). Realistic expectations of prepulse inhibition in translational models for schizophrenia research. Psychopharmacology *199*, 331–388.

64. Swerdlow, N., Geyer, M., and Braff, D. (2001). Neural circuit regulation of prepulse inhibition of startle in the rat: current knowledge and future challenges. Psychopharmacology *156*, 194–215.

65. Geyer, M.A., and Swerdlow, N.R. (1998). Measurement of Startle Response, Prepulse Inhibition, and Habituation. Current Protocols in Neuroscience *3*,.

66. Geyer, M.A., McIlwain, K.L., and Paylor, R. (2002). Mouse genetic models for prepulse inhibition: an early review. Mol Psychiatry *7*, 1039–1053.

67. Ashton, A.C., Volynski, K.E., Lelianova, V.G., Orlova, E.V., Van Renterghem, C., Canepari, M., Seagar, M., and Ushkaryov, Y.A. (2001). α-Latrotoxin, Acting via Two Ca2+-dependent Pathways, Triggers Exocytosis of Two Pools of Synaptic Vesicles. Journal of Biological Chemistry *276*, 44695–44703.

68. Volynski, K.E., Silva, J.-P., Lelianova, V.G., Atiqur Rahman, M., Hopkins, C., and Ushkaryov, Y.A. (2004). Latrophilin fragments behave as independent proteins that associate and signal on binding of LTXN4C. EMBO J *23*, 4423–4433.

69. Silva, J.-P., Lelianova, V., Hopkins, C., Volynski, K.E., and Ushkaryov, Y. (2009). Functional Cross-interaction of the Fragments Produced by the Cleavage of Distinct Adhesion G-protein-coupled Receptors. Journal of Biological Chemistry *284*, 6495–6506.

70. Capogna, M., Volynski, K.E., Emptage, N.J., and Ushkaryov, Y.A. (2003). The α-Latrotoxin Mutant LTX ^{N4C} Enhances Spontaneous and Evoked Transmitter Release in CA3 Pyramidal Neurons. J. Neurosci. *23*, 4044–4053.

71. Karczewski, K.J., Francioli, L.C., Tiao, G., Cummings, B.B., Alföldi, J., Wang, Q., Collins, R.L., Laricchia, K.M., Ganna, A., Birnbaum, D.P., et al. (2020). The mutational constraint spectrum quantified from variation in 141,456 humans. Nature *581*, 434–443.

72. De Rubeis, S., He, X., Goldberg, A.P., Poultney, C.S., Samocha, K., Cicek, A.E., Kou, Y., Liu, L., Fromer, M., Walker, S., et al. (2014). Synaptic, transcriptional and chromatin genes disrupted in autism. Nature *515*, 209–215.

73. Posner, M.I., and Dehaene, S. (1994). Attentional networks. Trends in Neurosciences *17*, 75–79.

74. McFarlane, H.G., Kusek, G.K., Yang, M., Phoenix, J.L., Bolivar, V.J., and Crawley, J.N. (2008). Autism-like behavioral phenotypes in BTBR T+tf/J mice. Genes Brain Behav *7*, 152–163.

75. Wu, W.-L., Cheng, S.-J., Lin, S.-H., Chuang, Y.-C., Huang, E.Y.-K., and Chen, C.-C. (2019). The Effect of ASIC3 Knockout on Corticostriatal Circuit and Mouse Self-grooming Behavior. Front. Cell. Neurosci. *13*, 86.

76. Lelyanova, V.G., Thomson, D., Ribchester, R.R., Tonevitsky, E.A., and Ushkaryov, Y.A. (2009). Activation of α-Latrotoxin Receptors in Neuromuscular Synapses Leads to a Prolonged Splash Acetylcholine Release. Bull Exp Biol Med *147*, 701–703.

77. Orlova, E.V., Rahman, M.A., Gowen, B., Volynski, K.E., Ashton, A.C., Manser, C., van Heel, M., and Ushkaryov, Y.A. (2000). Structure of alpha-latrotoxin oligomers reveals that divalent cation-dependent tetramers form membrane pores. Nat Struct Biol *7*, 48–53.

78. Ashton, A.C., Rahman, M.A., Volynski, K.E., Manser, C., Orlova, E.V., Matsushita, H., Davletov, B.A., van Heel, M., Grishin, E.V., and Ushkaryov, Y.A. (2000). Tetramerisation of α-latrotoxin by divalent cations is responsible for toxin-induced non-vesicular release and contributes to the Ca2+-dependent vesicular exocytosis from synaptosomes. Biochimie *82*, 453–468.

79. Heiming, R.S., Bodden, C., Jansen, F., Lewejohann, L., Kaiser, S., Lesch, K.-P., Palme, R., and Sachser, N. (2011). Living in a dangerous world decreases maternal care: A study in serotonin transporter knockout mice. Hormones and Behavior *60*, 397–407.

80. vom Saal, F.S., and Howard, L.S. (1982). The Regulation of Infanticide and Parental Behavior: Implications for Reproductive Success in Male Mice. Science *215*, 1270–1272.

81. Zafar, T., Naik, A.Q., and Shrivastava, V.K. (2018). Effect of cold stress on infanticide by female Swiss albino mice Mus musculus: a pilot study. J Anim Sci Technol *60*, 7.

82. Chen, M.-L., and Chen, C.-H. (2005). Microarray Analysis of Differentially Expressed Genes in Rat Frontal Cortex Under Chronic Risperidone Treatment. Neuropsychopharmacol *30*, 268–277.

83. Mao, Z., Bo, Q., Li, W., Wang, Z., Ma, X., and Wang, C. (2019). Prepulse inhibition in patients with bipolar disorder: a systematic review and meta-analysis. BMC Psychiatry *19*, 282.

84. Vysokov, N.V., Silva, J.-P., Lelianova, V.G., Ho, C., Djamgoz, M.B., Tonevitsky, A.G., and Ushkaryov, Y.A. (2016). The Mechanism of Regulated Release of Lasso/Teneurin-2. Front. Mol. Neurosci. *9*,.

85. Sando, R., Jiang, X., and Südhof, T.C. (2019). Latrophilin GPCRs direct synapse specificity by coincident binding of FLRTs and teneurins. Science *363*, eaav7969.

Figure1

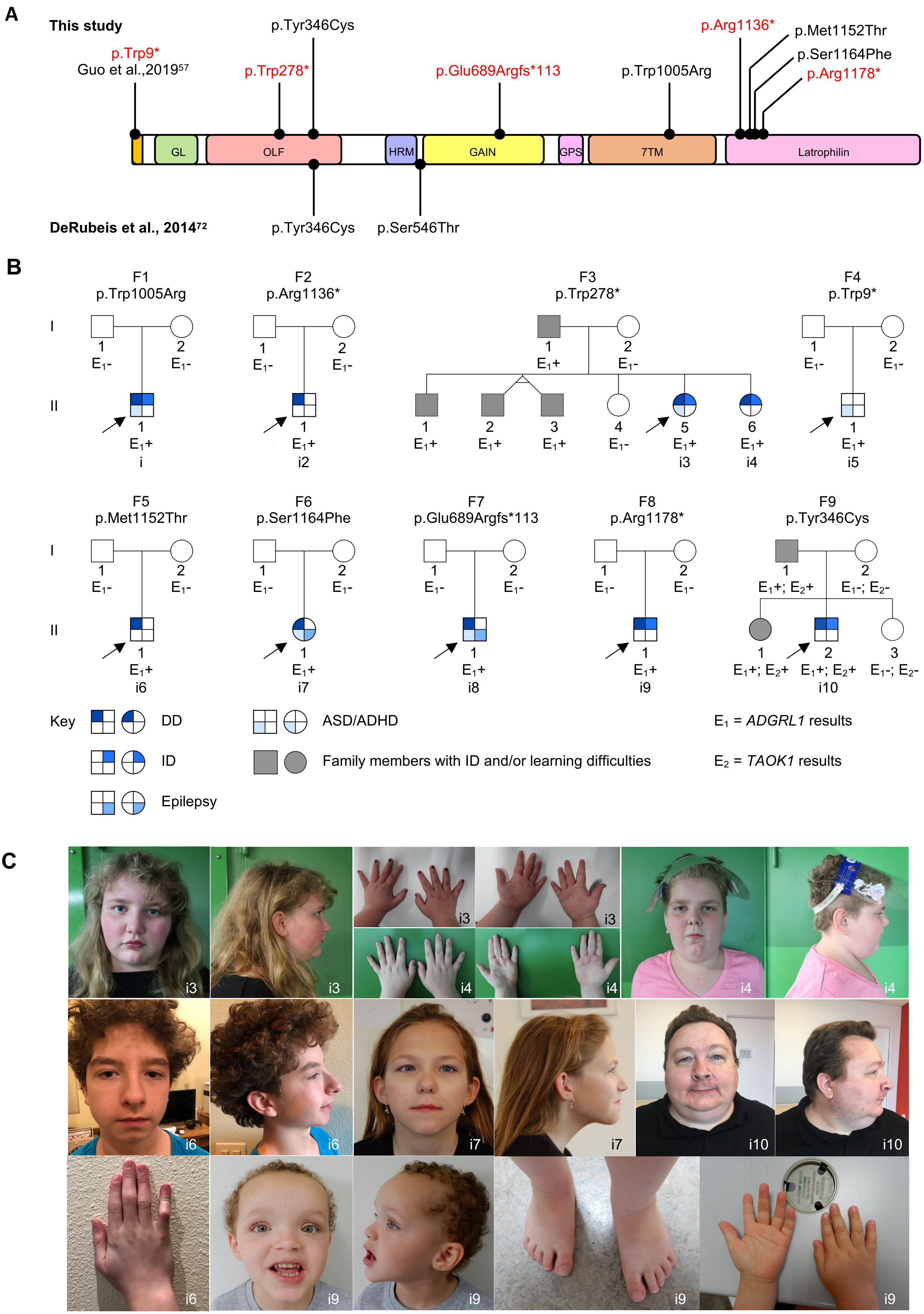
A
This study
p.Trp9*
Guo et al.,2019[57]
p.Trp278*
p.Tyr346Cys
p.Glu689Argfs*113
p.Trp1005Arg
p.Arg1136*
p.Met1152Thr
p.Ser1164Phe
p.Arg1178*
GL
OLF
HRM
GAIN
GPS
7TM
Latrophilin
DeRubeis et al., 2014[72]
p.Tyr346Cys
p.Ser546Thr
B
F1 p.Trp1005Arg
F2 p.Arg1136*
F3 p.Trp278*
F4 p.Trp9*
F5 p.Met1152Thr
F6 p.Ser1164Phe
F7 p.Glu689Argfs*113
F8 p.Arg1178*
F9 p.Tyr346Cys
I
II
E_1+
E_1-
E_1+; E_2+
E_1-; E_2-
i
i2
i3
i4
i5
i6
i7
i8
i9
i10
Key
DD
ID
Epilepsy
ASD/ADHD
Family members with ID and/or learning difficulties
E_1 = *ADGRL1* results
E_2 = *TAOK1* results
C
i3
i4
i6
i7
i9
i10

Figure 2

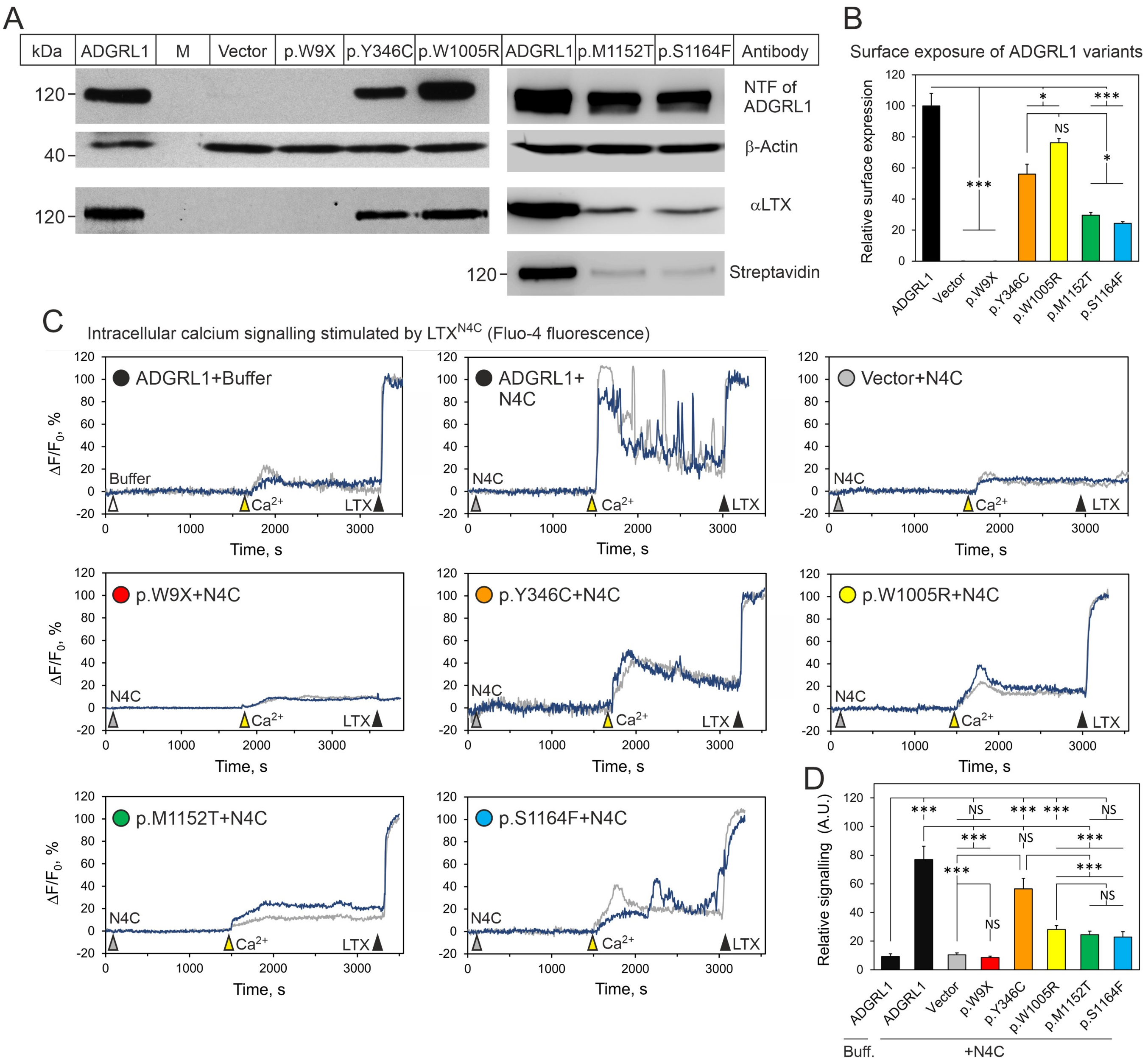
A
kDa
ADGRL1
M
Vector
p.W9X
p.Y346C
p.W1005R
ADGRL1
p.M1152T
p.S1164F
Antibody
120
NTF of ADGRL1
40
β-Actin
120
αLTX
120
Streptavidin
B
Surface exposure of ADGRL1 variants
Relative surface expression
0
20
40
60
80
100
120
***
*
***
NS
*
ADGRL1
Vector
p.W9X
p.Y346C
p.W1005R
p.M1152T
p.S1164F
C
Intracellular calcium signalling stimulated by LTX^N4C (Fluo-4 fluorescence)
● ADGRL1+Buffer
● ADGRL1+N4C
● Vector+N4C
● p.W9X+N4C
● p.Y346C+N4C
● p.W1005R+N4C
● p.M1152T+N4C
● p.S1164F+N4C
ΔF/F0, %
Time, s
Buffer
N4C
Ca2+
LTX
-20
0
20
40
60
80
100
120
0
1000
2000
3000
D
Relative signalling (A.U.)
0
20
40
60
80
100
120
***
NS
***
***
NS
***
NS
***
***
***
NS
***
NS
ADGRL1
ADGRL1
Vector
p.W9X
p.Y346C
p.W1005R
p.M1152T
p.S1164F
Buff.
+N4C

Figure 3

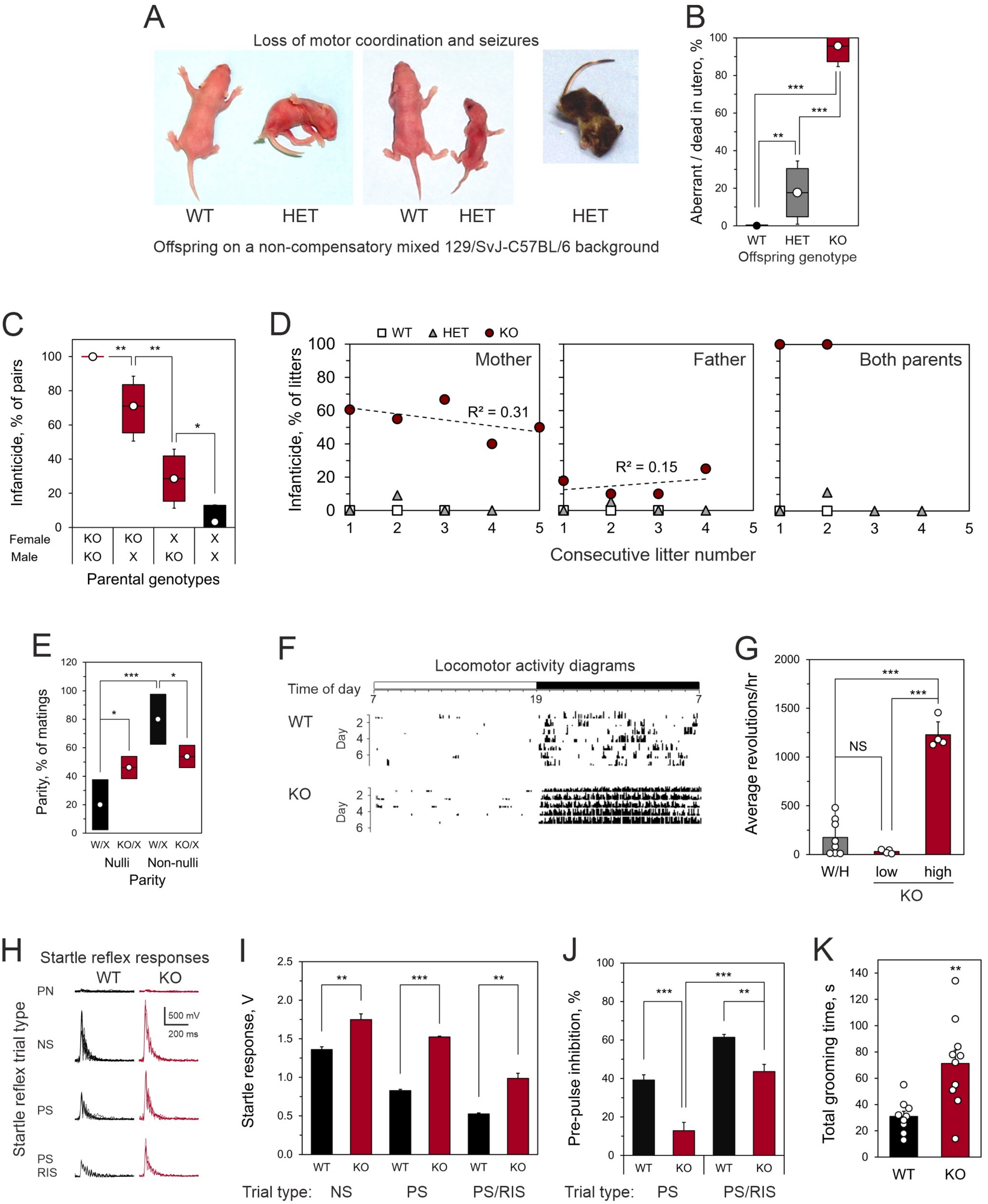
A
Loss of motor coordination and seizures
WT
HET
WT
HET
HET
Offspring on a non-compensatory mixed 129/SvJ-C57BL/6 background
B
Aberrant / dead in utero, %
100
80
60
40
20
0
***
***
**
WT
HET
KO
Offspring genotype
C
Infanticide, % of pairs
100
80
60
40
20
0
**
**
*
Female
Male
KO
KO
KO
X
X
KO
X
X
Parental genotypes
D
□ WT
▲ HET
● KO
Infanticide, % of litters
100
80
60
40
20
0
Mother
R² = 0.31
Father
R² = 0.15
Both parents
1
2
3
4
5
Consecutive litter number
E
Parity, % of matings
120
100
80
60
40
20
0
***
*
*
W/X
KO/X
W/X
KO/X
Nulli
Non-nulli
Parity
F
Locomotor activity diagrams
Time of day
7
19
7
WT
Day
2
4
6
KO
Day
2
4
6
G
Average revolutions/hr
2000
1500
1000
500
0
***
***
NS
W/H
low
high
KO
H
Startle reflex responses
WT
KO
Startle reflex trial type
PN
NS
PS
PS RIS
500 mV
200 ms
I
Startle response, V
2.5
2.0
1.5
1.0
0.5
0.0
**
***
**
WT
KO
WT
KO
WT
KO
Trial type:
NS
PS
PS/RIS
J
Pre-pulse inhibition, %
100
80
60
40
20
0
***
***
**
WT
KO
WT
KO
Trial type:
PS
PS/RIS
K
Total grooming time, s
140
120
100
80
60
40
20
0
**
WT
KO

Figure 4

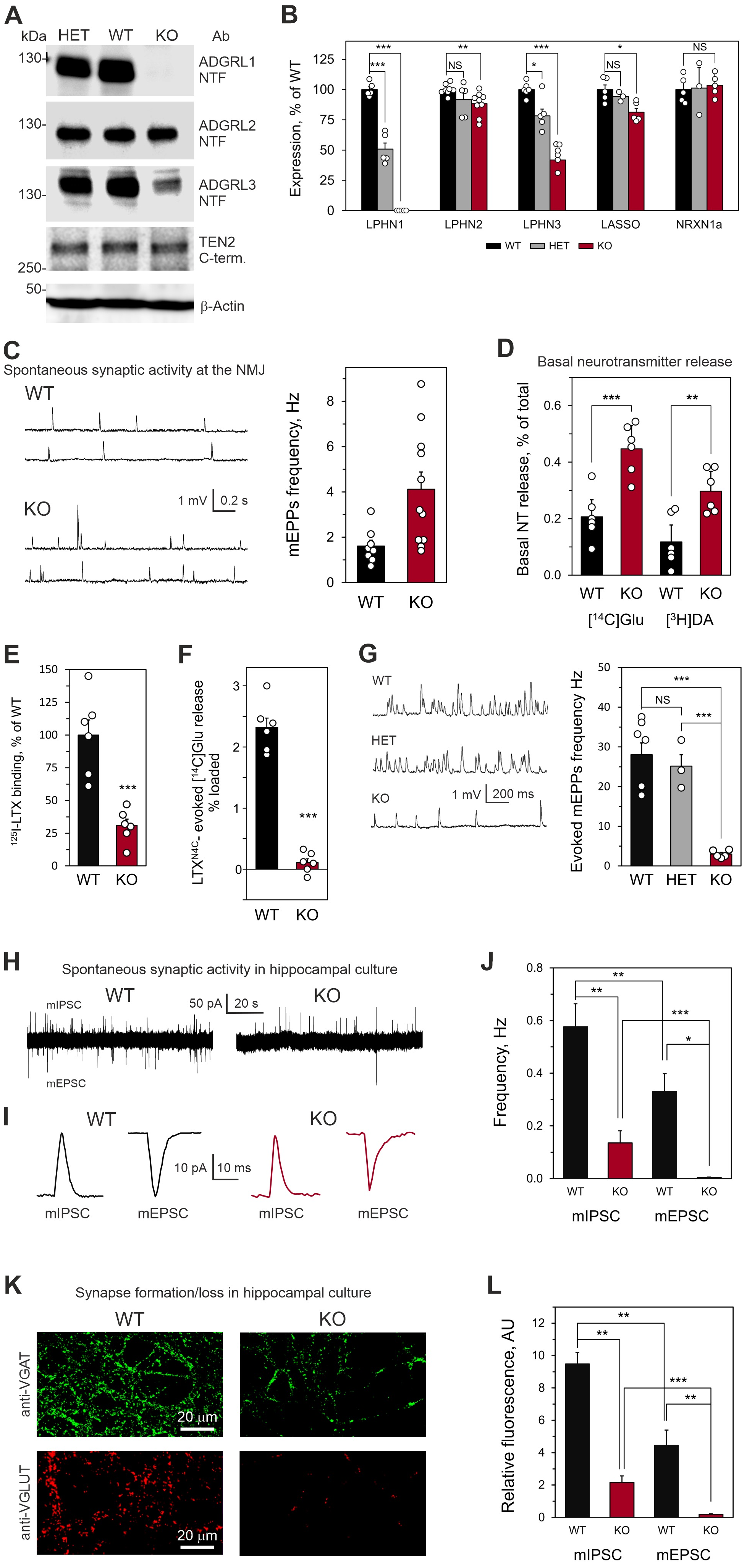
A
kDa
HET
WT
KO
Ab
130-
ADGRL1 NTF
130-
ADGRL2 NTF
130-
ADGRL3 NTF
250-
TEN2 C-term.
50-
β-Actin
B
Expression, % of WT
125
100
75
50
25
0
***
***
**
NS
***
*
*
NS
NS
LPHN1
LPHN2
LPHN3
LASSO
NRXN1a
WT
HET
KO
C
Spontaneous synaptic activity at the NMJ
WT
KO
1 mV
0.2 s
mEPPs frequency, Hz
8
6
4
2
0
WT
KO
D
Basal neurotransmitter release
Basal NT release, % of total
0.6
0.4
0.2
0.0
***
**
WT
KO
WT
KO
[14C]Glu
[3H]DA
E
125I-LTX binding, % of WT
150
125
100
75
50
25
0
***
WT
KO
F
LTXN4C- evoked [14C]Glu release % loaded
3
2
1
0
***
WT
KO
G
WT
HET
KO
1 mV
200 ms
Evoked mEPPs frequency Hz
50
40
30
20
10
0
***
NS
***
WT
HET
KO
H
Spontaneous synaptic activity in hippocampal culture
mIPSC
WT
50 pA
20 s
KO
mEPSC
I
WT
KO
10 pA
10 ms
mIPSC
mEPSC
mIPSC
mEPSC
J
Frequency, Hz
0.8
0.6
0.4
0.2
0.0
**
**
***
*
WT
KO
WT
KO
mIPSC
mEPSC
K
Synapse formation/loss in hippocampal culture
WT
KO
anti-VGAT
20 μm
anti-VGLUT
20 μm
L
Relative fluorescence, AU
12
10
8
6
4
2
0
**
**
***
**
WT
KO
WT
KO
mIPSC
mEPSC

Supplemental information

Supplemental Results

Conditional embryonic lethality of *Adgrl1*$^{-/-}$ mice

The heterozygous (HET) mice obtained from the chimeric founders on the 129/SvJ genetic background were backcrossed to a more robust C57BL/6 background. Subsequent interbreeding of the 129/SvJ-C57BL/6 mixed-background HET mice produced more than 100 WT and HET progeny, before the first KO pup was identified (Figure S2B-D). Using this animal, the backcrossing to C57BL/6 mice continued for eight additional generations. As a result, a permissive haplotype was achieved, on which many KO animals were born. However, after 324 matings, which produced 234 litters comprising more than 1270 mice born, the established colony still demonstrated non-Mendelian distribution of the *Adgrl1* allele in offspring, with *Adgrl1*$^{-/-}$ pups born at a clearly sub-Mendelian frequency (Figure S2E). Specifically, intercrossing two HET mice, on average, produced 1.9 times more WT than KO pups (Figure S2E, left). Likewise, when HET and KO animals were crossed, HET offspring were produced 2.4-fold more frequently than KO offspring (Figure S2E, right). Mating two *Adgrl1* nullizygous mice was also attempted, but out of 5 pairs only one was successful, producing two litters with 2-3 pups in each and killing them each time. HET animals (carrying one WT and one KO *Adgrl1*$^{-}$ allele) survived the gestation well, which indicated that the C57BL/6 genotype was at least partially compensatory, and that the disruptive mutant phenotype was recessive.

The observed paucity of KO progeny could be caused by several problems associated with the disruption of *Adgrl1*, such as low fertility of KO spermatozoa or developmental deficits in KO embryos. Therefore, we examined the relationship between parental genotypes and litter sizes and found that, on average, KO sires produced litters 20% smaller than those of WT sires, while KO dams produced litters 38% smaller than those of WT dams and 30% smaller than those of KO sires (Figure S2F). When considering the survival rate of *Adgrl1*$^{-/-}$ progeny in HET-KO pairs, we found that KO pups were born twice more frequently when the female was HET than if she was KO (Figure S2G). These results ruled out potential physiological or behavioral abnormalities of the *Adgrl1*-deficient males as the main reason for the underproduction of KO progeny and argued for litter size being dependent on the parents' genotypes, most likely as a consequence of abnormal embryonic lethality of KO conceptuses, especially when carried by KO dams. Indeed, dissection of several pregnant females, at gestation day 16, revealed embryo resorption sites indicative of *in utero* lethality at early stages of embryogenesis (not shown). Although the genotype of these dead embryos could not be established, the sub-Mendelian production of KO pups suggests that they were *Adgrl1*$^{-/-}$.

Behavioral abnormalities in *Adgrl1*$^{-/-}$ mice

While the colony was maintained on the mixed, non-compensatory 129/SvJ-C57BL/6 background, the HET pups born often showed neurodevelopmental abnormalities. In particular, more than 15% of HET pups were unable to move in a coordinated manner. The righting reflex was used to assess the level of arousal. At postnatal day four (P4), when this phenotype was most pronounced, the time required to flip from supine to prone position was 8.7 ± 0.7 s for WT pups and 42.5 ± 9.9 s for HET pups, with some affected animals being unable to right themselves at all and often spontaneously rolling over while attempting to crawl in the prone position. Inability to suckle was another consequence of uncoordinated locomotor activity and the main reason of severe malnourishment and underdevelopment of some HET pups (Figure 3A, middle). Two less affected HET animals survived until weaning, but then demonstrated neurological deficits, such as periodic arrests and focal seizures, especially when introduced into a novel environment (e.g. open space) (Figure 3A, right). These neurodevelopmental defects were not displayed by the WT animals (Figure 3B) and, upon outcrossing on a more permissive background, HET animals developed normally and revealed no behavioral or neurological deviations.

On the permissive C57BL/6 background, many KO animals successfully completed their development but demonstrated consistent infanticide. In 25 out of 27 cases, KO dams killed all the pups in the litter (Figure 3C). Live pups were sometimes observed before they were killed, but most offspring were killed within the first hour after birth. The dead neonates never showed milk spots, indicating that they had not been nursed by their mother. Each dead pup was either badly mauled or partially eaten, indicating that the mother (and sometimes the father) specifically aimed at killing each newborn. This behavior was consistent with a deliberate act of aggression rather than simple abandonment, lack of maternal care, passive cannibalism of the already dead offspring, or an attempt by the mother to protect herself by consuming her pups for nutrition in view of an outside danger (e.g. a predator). The almost immediate attack on the litter suggested an affective dysfunction, while the more delayed infanticide could also be driven by a cognitive impairment. These results suggested that pups' demands of food and comfort were perceived by the mother as an intensely intrusive stressful stimulus. The neonaticide did not depend on the pups' genotypes or number and, on average, occurred after 58% of parturitions, irrespective of the number of previous parturitions (Figure 3D). In other words, while many KO dams killed each litter, others attacked few of their litters, whereas some KO females only killed one out of several litters. This indicates that the stress caused by the presence of the litter could be conditioned by other factors, so that the anxiety did not always overwhelm the dam's sensory endurance, causing her to eliminate (kill) the source of distress only in ~60% of cases.

KO male mice killed their own offspring in 28.6% of cases (Figure 3C) and showed also no adaptation to subsequent litters, killing on average about 15.5% of litters after each parturition (Figure 3D). KO males, similar to KO females, were apparently unable to process intrusive environmental stimuli, but obviously the situation was less stressful for them than for females, leading to a lower prevalence of paternal infanticide. All pairs consisting of both KO parents killed their offspring (Figure 3C, D), and therefore KO-KO breeding pairs were normally avoided. Pairs, consisting of HET and/or WT animals on the *Adgrl1*$^{-/-}$-compensatory background, never killed their offspring (0 out of 35), while among 31 HET-HET inter-crosses, infanticide occurred only once. These results clearly demonstrate that only KO animals poorly tolerated stressful situations, but this phenotype was not sex-specific.

Supplemental figures and legends

Figure S1. Metadome intolerance score associated with missense variants. **A,** Variants reported in De Rubeis et al., 2014. **B,** Variants identified in our cohort. NM_001008701.2 transcript was used for this analysis.

Figure S2. Targeted disruption of *Adgrl1*. A, Schematic representation of the targeting event. Top, the original mouse *Adgrl1*. Middle, the targeting vector. Bottom, the resulting inactivated *Adgrl1*. The exons are shown as vertical bars. The brackets above and below indicate Eco RI fragments identified by Southern hybridization of the respective alleles; the numbered arrows represent the primers used for PCR-genotyping. The scale bar is provided on the right. **B**, Sub-Mendelian frequency of the *Adgrl1*$^{-/-}$ neonates in the offspring of HET-HET breeding pairs on a mixed 129/SvJ-C57BL/6 background. Blue bars with values, an expected Mendelian distribution of genotypes, in percent. Bright bars, the real genotypes distribution in offspring (n = 20 litters; 103 pups; $p < 4\text{x}10^{-6}$). **C**, Identification of the original and mutant *Adgrl1* alleles using PCR. M, MW markers. **D**, Western blot analysis of ADGRL1 and NRXN1 in WT and KO mouse brains. The image is representative of n = 6 experiments, which gave similar results. **E**, Persistent sub-Mendelian frequency of the *Adgrl1*$^{-/-}$ genotype in the mature colony on the C57BL/6 background. Color coding as in B. Left, genotypes of the progeny of HET-HET breeding pairs (n = 27 litters, 161 offspring; $p < 0.05$). Right, genotypes of the progeny of HET-KO breeding pairs (n = 97 litters, 558 offspring; $p < 3.4\text{x}10^{-10}$). **F**, Litter sizes as a function of parental genotypes (litter numbers n = 85 for KO male parent and n = 61 for KO female parent; $p < 1.5\text{x}10^{-5}$). In each case, the other parent was WT or HET. **G**, The proportion of KO pups in the offspring of HET-KO pairs, as a function of mother's genotype (HET dams: n = 74 litters, 445 offspring; KO dams: n = 23 litters, 113 offspring; $p < 0.001$). **H**, The amplitudes of spontaneous mEPPs do not differ in WT and KO mice at rest, as in Figure 4C ($p > 0.05$; WT, n = 8; KO, n = 11). **I**, The amplitudes of LTX^{N4C}-evoked mEPPs are similar at the NMJs of WT and HET mice, as in Figure 4G (WT, n = 6; HET, n = 3; KO, n = 5 independent animals). **J**, The amplitudes of mIPSCs and mEPSCs in WT and KO neuronal cultures, as in Figure 4H (n = 28 for each condition).

Supplemental Methods

Exome sequencing and bioinformatics

Several approaches were utilized according to each institution.

Dijon. Libraries of genomic DNA samples were prepared using the Twist Human Core Exome kit (Twist Biosciences, San Francisco, CA), and were sequenced on a NovaSeq 6000 instrument (Illumina, San Diego, CA) according to the manufacturer’s recommendations for paired-end 151-bp reads. A mean depth of 86.96 x was reach and 97.2 % of the refseq exons were covered at least by 10 reads.

Variants were identified using a computational platform of the FHU Translad, hosted by the University of Burgundy Computing Cluster (CCuB). Raw data quality was evaluated by FastQC software (v0.11.4). Reads were aligned to the GRCh37/hg19 human genome reference sequence using the Burrows-Wheeler Aligner (v0.7.15). Aligned read data underwent the following steps: (a) duplicate paired-end reads were removed by Picard software (v2.4.1), and (b) base quality score recalibration was done by the Genome Analysis Toolkit (GATK v3.8) Base recalibrator. Using GATK Haplotype Caller, Single Nucleotide Variants with a quality score >30 and an alignment quality score >20 were annotated with SNPEff (v4.3). Rare variants were identified by focusing on nonsynonymous changes present at a frequency less than 1% in the GNOMAD database. Copy Number Variants were detected using xHMM (v1.0) and were annotated using in-house python scripts. They were filtered regarding their frequency in public databases (DGV, ISCA, DDD).

Paris. Sequencing libraries were prepared using the KAPA HyperExome (Roche, Basel, Switzerland) and sequenced as 75-bp paired-end reads on the Nextseq 500 platform (Illumina, San Diego, CA, USA). Reads were processed following a standard analysis pipeline at the Pitié-Salpêtrière University Hospital. Overall sequencing and quality was assessed with FastQC v0.11.8, the reads were then aligned to the reference human genome sequence (hg19) using the Burrows-Wheeler Aligner BWA-mem v0.7.17, the alignment files were sorted and indexed using Samtools v1.9, and Sambamba v0.7.0 was used to flag duplicates. Variants were called using GATK Software v4.1.4. Multi-allelic variants were split and indels were normalized using vt 0.57721. Variants were annotated with Variant Effect Predictor (v105), and filtered according to population occurrence (gnomAD v2 and v3), impact, and segregation. Copy Number Variants were called using an in-house algorithm. In brief, depth of coverage of a genomic region was compared across the co-sequenced individuals in the same library (n=12). They were analyzed according to population databases (DGV) and co-occurrence in the same run.

GeneDx. Exome sequengin was performed as previously described in Retteret et al.[1] In summary, using genomic DNA from the proband and parents, the exonic regions and flanking splice junctions of the genome were captured using the IDT xGen Exome Research Panel v1.0 (Integrated DNA Technologies, Coralville, IA). Massively parallel (NextGen) sequencing was done on an Illumina system with 100bp or greater paired-end reads. Reads were aligned to human genome build GRCh37/UCSC hg19, and analyzed for sequence variants using a custom-developed analysis tool. Reported variants were confirmed, if necessary, by an appropriate orthogonal method in the proband and, if submitted, in selected relatives. Additional sequencing technology and variant interpretation protocol has been previously described**. The general assertion criteria for variant classification are publicly available on the GeneDx ClinVar submission page (http://www.ncbi.nlm.nih.gov/clinvar/submitters/26957/)"

Aachen. For whole exome sequencing (WES), a DNA sample from the index patient was enriched using the Lotus™ DNA Library preparation kit (IDT, Coralville, Iowa) according to the manufacturers protocol. The exome library was sequenced on a NextSeq500 Sequencer with 2 × 75 cycles on a high-output flow cell (Illumina, San Diego, CA). FastQ-files were generated with bcl2fastq2 (Illumina). The alignment and variant calling was done using the SeqMule pipeline (v1.2.6). For variant detection, three different variant callers were used (GATKLite UnifiedGenotyper, SAMtools, FreeBayes consensus) and variants detected by at least two variant callers were taken for further assessment. Annotation and prioritization of variants were performed using KGGSeq (v1.0, 20/Jun./2018).

Synonymous variants and variants with a minor allele frequency (MAF) higher than 0.75% in public databases (i.e., gnomAD, EXAC, 1000 GP, ESP) were excluded.

Huston. Exome sequencing was performed as previously described in Yang et al.[2]

Supplemental references

1. Retterer, K., Juusola, J., Cho, M.T., Vitazka, P., Millan, F., Gibellini, F., Vertino-Bell, A., Smaoui, N., Neidich, J., Monaghan, K.G., et al. (2016). Clinical application of whole-exome sequencing across clinical indications. Genet Med *18*, 696–704.

2. Yang, Y., Muzny, D.M., Xia, F., Niu, Z., Person, R., Ding, Y., Ward, P., Braxton, A., Wang, M., Buhay, C., et al. (2014). Molecular findings among patients referred for clinical whole-exome sequencing. JAMA *312*, 1870–1879.